Photoreceptor-Mimetic Microflowers for Restoring Light Responses in Degenerative Retina through a 2D Nanopetal/Cell Biointerface

Gerile Oudeng, Seema Banerjee, Qin Wang, Ding Jiang, Yadi Fan, Honglian Wu, Feng Pan, and Mo Yang**

Retinitis pigmentosa is the main cause of inherited human blindness and is associated with dysfunctional photoreceptors (PRs). Compared with traditional methods, optoelectronic stimulation can better preserve the structural integrity and genetic content of the retina. However, enhancing the spatiotemporal accuracy of stimulation is challenging. Quantum dot-doped $ZnIn_2S_4$ microflowers (MF) are utilized to construct a biomimetic photoelectric interface with a 0D/3D heterostructure, aiming to restore the light response in PR-degenerative mice. The MF bio interface has dimensions similar to those of natural PRs and can be distributed within the curved spatial region of the retina, mimicking cellular dispersion. The soft 2D nano petals of the MF provide a large specific surface area for photoelectric activation and simulate the flexibility interfacing between cells. This bio interface can selectively restore the light responses of seven types of retina ganglion cells that encode brightness. The distribution of responsive cells forms a pattern similar to that of normal mice, which may reflect the generation of the initial "neural code" in the degenerative retina. Patch-clamp recordings indicate that the bio interface can induce spiking and postsynaptic currents at the single-neuron level. The results will shed light on the development of a potential bionic subretinal prosthetic toolkit for visual function restoration.

1. Introduction

Retinitis pigmentosa (RP) is a main cause of inherited human blindness globally, manifesting in adolescents and young adults and characterized by degeneration of the photoreceptors (rods and cones) in the retina.[1] Its prevalence is reported as 1 in 3000 to 5000 individuals, with close to 2 million people affected worldwide.[2] Photoreceptors convert light into electrical signals, which then pass through interneurons to retinal ganglion cells (RGCs), where the visual information is ultimately coded and transmitted to the brain for generating images.[3a,b] The image received is blurred or completely unseen when the photoreceptor cells disappear due to retinal degeneration. Although much effort has been made to restore visual function, including electrical and optogenetic stimulation, apart from Luxturna (voretigene neparvovec-rzyl) gene therapy for inherited retinal dystrophies,[4] no suitable clinical

---

G. Oudeng, D. Jiang, Y. Fan, H. Wu, M. Yang
Department of Biomedical Engineering
The Hong Kong Polytechnic University
Hung Hom, Kowloon, Hong Kong SAR 999077, P. R. China
E-mail: mo.yang@polyu.edu.hk

G. Oudeng
Department of Hematology and Oncology
Shenzhen Children's Hospital
Shenzhen 518033, P. R. China

S. Banerjee, Q. Wang, F. Pan
School of Optometry
Research Centre for SHARP Vision (RCSV)
The Hong Kong Polytechnic University
Hung Hom, Kowloon, Hong Kong SAR 999077, P. R. China
E-mail: fengpan@polyu.edu.hk

The ORCID identification number(s) for the author(s) of this article can be found under https://doi.org/10.1002/smll.202400300

DOI: 10.1002/smll.202400300

S. Banerjee
Department of Ophthalmology and Genetics Medicine
Wilmer Eye Institute
Johns Hopkins University
Baltimore 22203, USA

S. Banerjee, Q. Wang, F. Pan
Centre for Eye and Vision Research (CEVR)
17W Hong Kong Science Park, Hong Kong China

Q. Wang
University of Health and Rehabilitation Sciences
o. 369, Qingdao National High-Tech Industrial
Development Zone, Shandong Province China

D. Jiang
Jiangsu Key Laboratory of Advanced Catalytic Materials and Technology
School of Petrochemical Engineering
Changzhou University
Changzhou 213159, P. R. China

F. Pan, M. Yang
Hong Kong Polytechnic University Shenzhen Research Institute
Shenzhen China

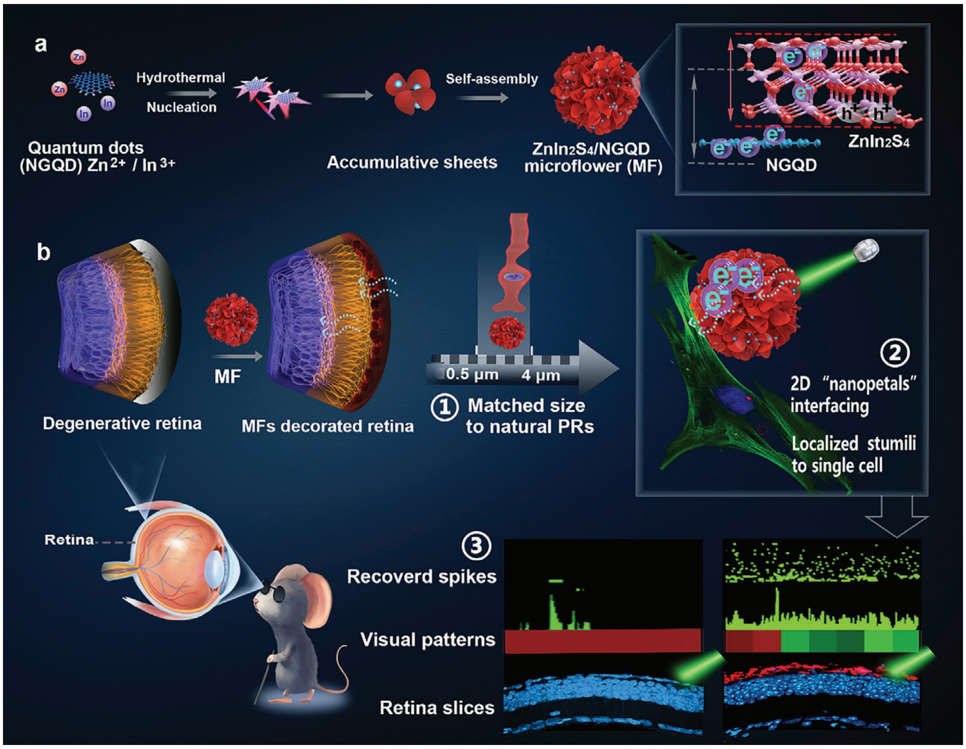

Figure 1. Retina–$ZnIn_2S_4$/NGQD-based MF biointerface. a) Fabrication of the $ZnIn_2S_4$/NGQD microflowers. b) The degenerative retina of a P66 Rd 10 mouse model lacks photoreceptors and has deficient firing under light stimuli. The degenerated photoreceptor layer (rod and cone cells) in the blind retina is replaced by microinjection of $ZnIn_2S_4$/NGQD MFs as a photoelectrical biointerface.

therapy has yet been developed. Electrical stimulation approaches, such as photovoltaic subretinal prostheses, which involve implanting and penetrating electrodes, suffer from potential invasive effects.[5a,b,c] Although optogenetic retinal stimulation is considerably more cell-friendly, there are still some concerns about the safety of viral vectors for exogenous light-sensitive protein delivery and the relatively moderate sensitivity of light-sensitive proteins to stimuli at physiological light levels.[6a,b,c] Ideally, stimulation of retinal cells should not interfere with either the genetic content or the structural integrity of cells.[7a,b]

Recently, the development of optoelectronic materials with wire-free structures and self-powering autonomy to interface with the blind retina has provided a new alternative for vision recovery.[8a,b,c] Various optoelectronic materials, such as semiconductor silicon[9a,b,c] and conducting polymers,[10a,b,c] have been used to generate artificial photoreceptors for retinal prostheses. However, rigid photoelectric substrates or films are highly invasive and can be used ex vivo. Some nanoparticles excel in minimal invasiveness, but they are prone to be taken up by cells, making it difficult to form seamless interfaces with the cell membrane and facilitate direct optoelectronic transmission.[11] The high spatiotemporal resolution of natural retinal images is based on the function of cone photoreceptor cells, with diameters of 0.5–4 μm, to transfer input to the visual cortex.[12a,b] Extensive research on constructing a PR-mimetic biomaterial that can disperse in the spherical space of retinal, generate a flexible interface to match cell hardness, and improve the precise transmission of photoelectrical signals to micron-sized cells, is still lacking.

Among various photoresponsive materials targeting the goal of cell-like biointerface, zinc indium sulfide ($ZnIn_2S_4$) microflowers (MFs), composed of ultrathin "petals" with nanosheets, exhibit high surface areas for photoactivation, excellent biocompatibility, and similar diameters to natural photoreceptor cells.[13a,b] The flower-like surface roughness of $ZnIn_2S_4$ may enhance interfacing efficiency with innate retinal cells, which is critical for the recovery of visual function. In addition, the coupling of nanomaterials with various bandgaps to form a heterostructure can enhance light utilization across the entire visible spectrum and improve photocurrent conversion efficiency for potential photostimulation. Quantum dots are excellent optical nanomaterials that have received considerable attention since being awarded the Nobel Prize in Chemistry in 2023.[14] Nitrogen-doped graphene quantum dots (NGQDs) have both graphene and 0D structures with good conductivity and unique surface effects, where the charge carriers easily diffuse from the inside to the surface.[15] Thus, coupling NGQDs with $ZnIn_2S_4$ MFs is expected to enhance the photocurrent conversion efficiency and the interaction between cells and materials.[16a,b]

In this study, we developed heterostructural 0D/3D microflowers based on $ZnIn_2S_4$/NGQD to create a biointerface in a retina-degenerated (P66 rd 10) RP mouse model through microinjection (**Figure** 1a). Under visible light excitation, charge/hole separation was triggered on the $ZnIn_2S_4$/NGQD MFs, to induce a photocurrent at the biointerface, stimulating the remaining bipolar cells (BCs) and further transferring the electrical signals to RGCs in the remaining retinal circuit (Figure 1b). The light responses of seven major ON or OFF RGCs for brightness coding

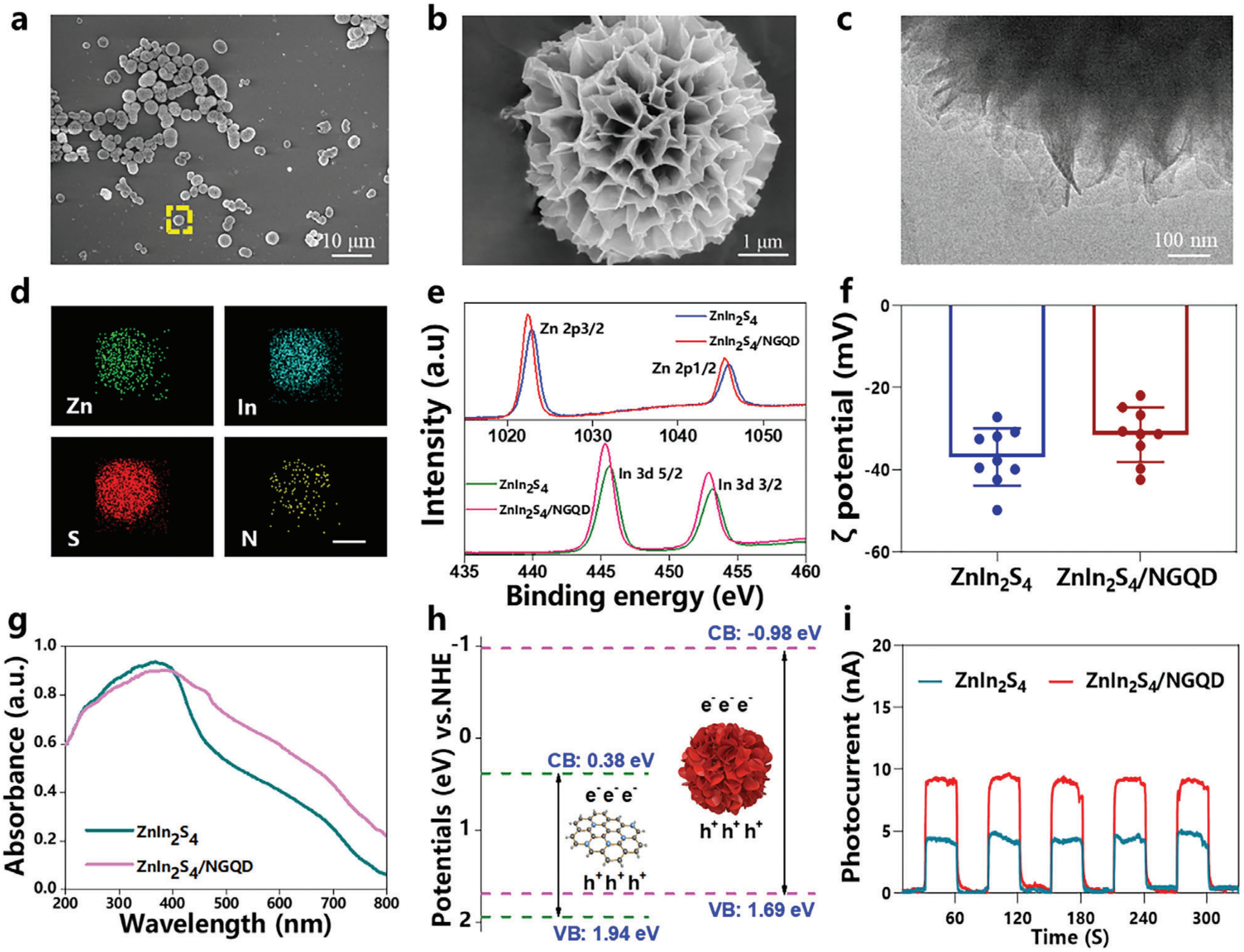

Figure 2. Fabrication of $ZnIn_2S_4$/NGQD MF. a) SEM image of as-prepared $ZnIn_2S_4$/NGQD MFs. b) Enlarged SEM image for one $ZnIn_2S_4$/NGQD MF with flower-like structure. c) High-resolution SEM image of 2D nanosheets on the flower-like structure. d) Element mapping of a single $ZnIn_2S_4$/NGQD MF. e) High-resolution XPS spectra of Zn 2p and In 3d for $ZnIn_2S_4$ and $ZnIn_2S_4$/NGQD MF. f) Zeta-potentials of $ZnIn_2S_4$ and $ZnIn_2S_4$/NGQD MFs. g) UV-vis diffuse reflectance spectrum of $ZnIn_2S_4$ and $ZnIn_2S_4$/NGQD MFs. h) Relative energy levels and light-induced charge transfer process of $ZnIn_2S_4$ and NGQD. i) Photogenerated currents of $ZnIn_2S_4$ and $ZnIn_2S_4$/NGQD microflowers under green light irradiation.

were successfully restored. These light-induced responses persisted even when inner retinal activation from residual photoreceptors (PRs) to bipolar cells (BCs) was blocked, indicating that the individual transmittance was formed from the MF biointerfaces to BCs. More interestingly, the RGCs activated by the MF biointerface showed a similar pattern to that of a normal retina, indicating the generation of an initial "neural code" in the RP mouse model.[17] Due to the minimally invasive nature of microinjection, effective interfacing with the retina, and potential for high spatial resolution, this work highlights the promise of the MF biointerface in restoring the retinal phototransduction process.

2. Results and Discussion

2.1. Fabrication of $ZnIn_2S_4$/NGQD MFs

The hybrid cell-like $ZnIn_2S_4$/NGQD MFs were synthesized using a one-pot hydrothermal approach with a mixture of $Zn(NO_3)_2$, $In(NO_3)_3$, and NGQDs, in which nucleation occurred first, followed by aggregation and re-crystallization (Figure 1a).[18a,b] The as-prepared NGQDs exhibited an average diameter of 2–5 nm with a crystalline structure, as revealed by transmission electron microscopy (TEM) imaging (Figure S1, Supporting Information). The shape of $ZnIn_2S_4$/NGQD MFs, analyzed by scanning electron microscopy (SEM), showed a flower-like structure with an average size of 2–5 μm (**Figure 2**a; Figure S2, Supporting Information), which is close to the natural diameter of rods (≈2 μm) and cones (0.5–4 μm).[19] In these "flowers", numerous thin nanosheets form the 2D nanopetals, providing a larger surface area to achieve higher charge transfer capability and more efficient interaction with retinal tissues (Figure 2b,c; Figure S3, Supporting Information). We synthesized $ZnIn_2S_4$ in various morphologies, including granular, nanosheet, semi-flower, and flower-like structures, by varying the synthesis time and precursor reactants.[20a,b] The results indicated that the products with nanosheet and flower-like morphologies exhibited strong and comparable photocurrent responses. (Figure S4, Supporting

Information). However, nanosheets tend to aggregate and restack, obscuring their surface area and active sites We selected the 3D flower-like structure as the optimized product due to its high photocurrent, the ease of inserting dopant materials between the nanosheet layers, and its favorable morphology for forming a close biointerface with cells.[15,21] To determine the appropriate mass ratio of doped NGQDs, $ZnIn_2S_4$ doped with 1.14, 3.46, 4.71 wt.% NGQDs addition was analyzed via a photoluminescence (PL) spectrum. $ZnIn_2S_4$ doped with 3.46 wt.% NGQDs was determined to be the optimum ratio because it exhibited the lowest PL intensity, indicating the lowest charge recombination[22] (Figure S5, Supporting Information).

Energy-dispersive X-ray (EDX) elemental mapping of the $ZnIn_2S_4$/NGQD MFs showed a uniform distribution of the main elements Zn, In, S, and N, indicating uniform doping of NGQD in the microflowers (Figure 2d). X-ray diffraction (XRD) analysis was performed to confirm the successful formation of $ZnIn_2S_4$/NGQD MFs (Figure S6, Supporting Information). High-resolution X-ray photoelectron spectroscopy (XPS) revealed slight shifts in the binding energies associated with Zn 2p and In 3d in $ZnIn_2S_4$ and $ZnIn_2S_4$/NGQD, to 452/445 eV and 1045/1022 eV, respectively (Figure 2e).[23a,b] The ζ potential of $ZnIn_2S_4$/NGQD MFs slightly shifted from −36.8 to −31.4 mV (Figure 2f), which demonstrated good hydrophilicity to facilitate the interaction with retinal tissues in the physiological environment.[24] In Kelvin probe force microscopy (KPFM) analysis, the $ZnIn_2S_4$/NGQD MFs showed a large contact potential difference (CPD), which might be attributed to the influence of nitrogen heteroatoms in graphene quantum dots, resulting in the redistribution of charges within the framework (Figure S7, Supporting Information).[25]

UV-vis diffuse reflectance spectra of $ZnIn_2S_4$ and $ZnIn_2S_4$/NGQD showed that NGQD extended the absorption range of $ZnIn_2S_4$ up to 800 nm, indicating the enhanced visible-light absorbance of $ZnIn_2S_4$/NGQD (Figure 2g). The optical band gaps of $ZnIn_2S_4$ and $ZnIn_2S_4$/NGQD analyzed by Tauc plots were 2.59 and 2.18 eV, respectively, showing the bandgap was shortened by NGQD doping (Figure S8, Supporting Information). Positive slopes in the Mott-Schottky plots of both samples confirmed the typical n-type characteristics of the prepared $ZnIn_2S_4$/NGQD MFs (Figure S9a, Supporting Information).[26a,b] In the Nyquist plots of electrochemical impedance spectra (EIS), $ZnIn_2S_4$/NGQD exhibited a smaller semicircle, indicating that the heterojunction promoted charge separation and interfacial charge transfer.[27] (Figure S9b, Supporting Information) Ultrafast transient absorption spectroscopy is employed to probe the dynamic process of the MF samples in real-time (Figure S10, Supporting Information). A 350 nm pump laser was applied to excite electrons from the valence band, while transient absorption kinetics data of the sample were collected within the visible range (500–800 nm). The $ZnIn_2S_4$/NGQD, with an average relaxation time (τ) of 387 ps, exhibited a longer τ compared to $ZnIn_2S_4$ alone, which might suggest efficient electron transfer between the components.[27,28] Figure 2h shows the relative energy levels and light-induced charge transfer processes of $ZnIn_2S_4$ and NGQD, which provide the basis for the photoelectrical response of the hybrid $ZnIn_2S_4$/NGQD MFs.

The photoconversion properties of the $ZnIn_2S_4$ and $ZnIn_2S_4$/NGQD MFs were demonstrated by photocurrent measurement under green light irradiation (520 nm) (Figure 2i). The typical substrate size was 1 cm^2 with a deposition concentration of 4 mg mL^{-1}. Upon illumination with green light, both $ZnIn_2S_4$ and $ZnIn_2S_4$/NGQD MFs exhibited a significant and immediate increase in photocurrent compared to the dark state. The photocurrent returned to baseline levels once the light was turned off. The photogenerated currents of the $ZnIn_2S_4$/NGQD MFs under green light irradiation were about 2 times that of $ZnIn_2S_4$ MFs. Under full visible light irradiation, the photogenerated currents of the $ZnIn_2S_4$/NGQD MFs were approximately 3.75 times that of the $ZnIn_2S_4$ MFs (Figure S11, Supporting Information). The distinct enhancement of the photocurrent may be attributed to the improved carrier separation and charge transfer rate due to NGQD coupling.[29] The photocurrents generated by $ZnIn_2S_4$/NGQD MFs under near UV, blue, and green wavelengths showed average magnitudes of 58.1, 15.2, and 9.8 nA, respectively (Figure S12, Supporting Information). The response of photoreceptors to green light plays a significant role in the process of retinitis pigmentosa (RP), with green light offering advantages in penetration and safety compared to other wavelengths.[30] In the following photo-stimulation experiments, green light with the lowest photocurrent was used as a demonstration of the feasibility of photostimulation of degenerative retinas.

Ensuring the long-term photoelectrical stability of $ZnIn_2S_4$/NGQD in a physiological retinal environment is crucial for providing consistent and reliable stimulation of retinal activity. The synthesized $ZnIn_2S_4$/NGQD MFs were incubated in phosphate-buffered saline (PBS), specific culturing medium for retinal ganglion cells (661 W RGCs), and the bicarbonate buffer used for retina maintaining, respectively. The photoelectrochemical current for each group remained stable under green light excitation, with no significant photocurrent response failure observed (Figure S13, Supporting Information). The non-degradable nature of $ZnIn_2S_4$/NGQD MFs might benefit its structural integrity and performance stability.[31a,b] From the outset of this study, it was surmised that the micron-sized flower-like hierarchical $ZnIn_2S_4$/NGQD would not be endocytosed by cells, but rather should be capable of forming close contacts and a high-surface-area with the cells. To test this hypothesis, the $ZnIn_2S_4$/NGQD MFs were cultured with neuronal PC12 cells. The $ZnIn_2S_4$/NGQD MFs attached well to the neuron cell membrane surface for up to 5 days of incubation, generating a good biointerface for neurostimulation (**Figure 3**). SEM imaging showed that the extracellular matrix and plasma membrane of the neuronal cells conformed to the flower-like structure of $ZnIn_2S_4$/NGQD, revealing effective interfaces without cell internalization (Figure 3a,b). PC12 cells spread over the flower-like structures of the MFs during cell culture (Figure 3c), with uncompromised viability, as verified by Calcein AM/PI staining assays (Figure S14, Supporting Information). Compared to rigid substrates, this MF biointerface with granular shapes has a larger surface area for interacting with cells in the neural network.[32] Confocal fluorescence imaging and cross-section confocal fluorescence imaging also indicated close interactions between the typical cytoskeleton protein of cells, filamentous actin (F-actin) of neuron cells (green), and the surface of the $ZnIn_2S_4$/NGQD MFs (red) to form a tight interface (Figure 3d–g).

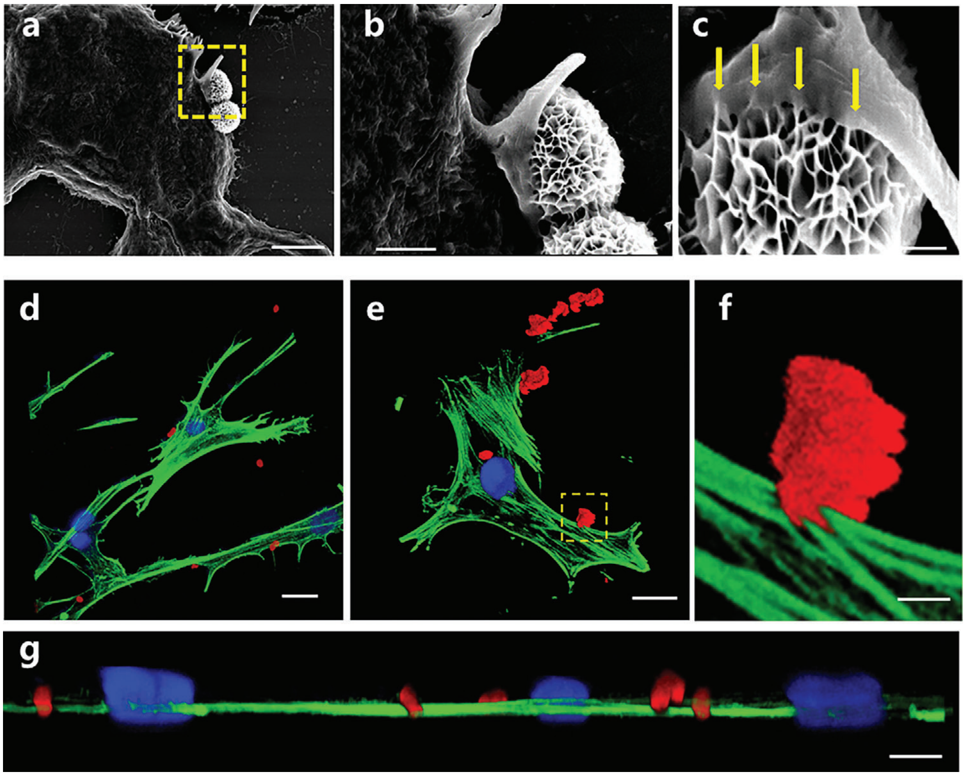

Figure 3. Interaction between $ZnIn_2S_4$/NGQD MFs and neuron cells. a-c) SEM images of attachment of $ZnIn_2S_4$/NGQD MFs on the PC12 neuron cell surface. MFs were conspicuously engulfed by the neuronal cells. Scale bar: a) 5 µm, b) 1 µm, and c) 200 nm. d-f) Confocal fluorescence microscopy images of interaction between $ZnIn_2S_4$/NGQD MFs and PC12 neuron cells. MFs (intrinsic red fluorescence) closely attach to the neuron cell surface. Scale bar: d) 10 µm, e) 5 µm and f) 1 µm. g) Lateral projection of z-stack confocal fluorescence image of PC12 neuron cells incubated with $ZnIn_2S_4$/NGQD MFs. Scale bar: 5 µm.

2.2. In Vitro and In Vivo Biocompatibility of $ZnIn_2S_4$/NGQD MFs

The in vitro and in vivo biocompatibility of the implanted $ZnIn_2S_4$/NGQD MFs could provide crucial evidence to evaluate their potential in biomedical applications. First, we characterized the cell viability of retinal ganglion cells and retinal pigment epithelial cells (RPECs) co-cultured with $ZnIn_2S_4$/NGQD MFs by live/dead assays and flow cytometry. The cell viability of RGCs and RPECs maintained around 90% when co-cultured with the $ZnIn_2S_4$/NGQD MFs for 24 and 48 h (**Figure** 4a,b). To evaluate the in vivo biocompatibility of $ZnIn_2S_4$/NGQD MFs, we subretinally injected the particles into the wide-type (WT) mice and then analyzed the expression of pro-inflammatory cytokines expression in their serum. No significant elevation in tumor necrosis factor-alpha (TNF-α) and interleukin-6 (IL-6) levels was observed in WT mice 48 h after MF injection ($p > 0.05$, $n = 3$). (Figure 4c). Furthermore, the MFs exhibited relatively low hemolytic activity (<5%), indicating their high safety for blood (Figure 4d). Additionally, no obvious organ damage to the heart, liver, spleen, lungs, or kidneys was observed in the mice, as confirmed by the hematoxylin and eosin (HE) staining images. (Figure 4e). The effect of $ZnIn_2S_4$/NGQD MFs on intact retinal regions was then investigated using hematoxylin and eosin (HE) staining for retinal slices, along with immunohistochemical staining for typical pre-inflammation biomarkers in the retinas. There were no significant changes for the PR cell counts and outer nuclear layer (ONL) thickness between the WT retinas with and without $ZnIn_2S_4$/NGQD MFs injection, which indicated the MFs implantation did not induce organ damage in the retinal region (Figure S15, Supporting Information). Typical markers of the proinflammatory response, including glial fibrillary acidic protein (GFAP) and ionized calcium-binding adapter molecule-1 (IBA1) are assessed in Figure S16 (Supporting Information).[8c] The results showed that MFs injection did not induce a significant increase in GFAP and IBA1 expression ($p > 0.05$, $n = 3$), which indicated the in vivo biosafety of the MFs in retinas. The systematic biosafety assays above successfully demonstrated the good in vivo biocompatibility of MFs.

2.3. Formation of the MF Biointerface and Photostimulation of RGCs in P66 Rd10 Mouse

The formation of a $ZnIn_2S_4$/NGQD based MF biointerface and its capability to induce light-dependent neuronal activation in the RGCs of degenerative retinas from P66 rd10 mice were systematically tested. $ZnIn_2S_4$/NGQD MFs and glass microspheres (MSs) were microinjected into the subretinal space of degenerative retinas. Retinas from WT mice were used as normal controls. Five days after microinjection, the $ZnIn_2S_4$/NGQD MFs were closely attached to the retinal layer to form an MF–retina biointerface. SEM revealed that $ZnIn_2S_4$/NGQD MFs formed close contact

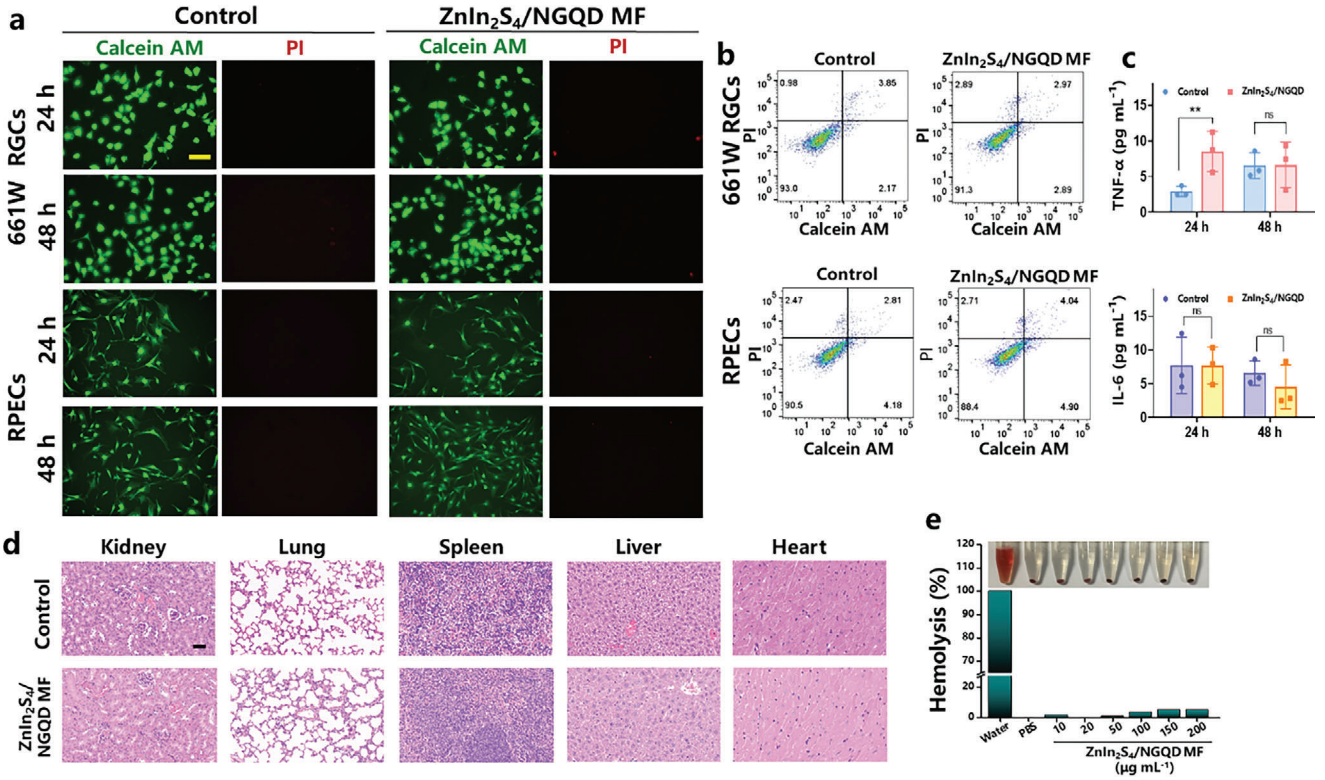

Figure 4. a,b) Calcein AM/PI fluorescence staining and flow cytometry analysis of 661 W RGCs and RPECs treated with MFs for 24 and 48 h (Scale bar: 100 μm); c) ELISA assay of TNF-*α* and IL-6 expression for WT mice serum treated with $ZnIn_2S_4$/NGQD MFs ($n = 3$); d) HE staining of main organs of mice treated with PBS (control) and MFs (Scale bar: 50 μm); e) Image and analysis of hemolysis rate of mice blood treated with MFs (10–200 μg mL^{-1}).

with the retina along the surface of the retinal layer (**Figure 5**a). Some $ZnIn_2S_4$/NGQD MFs were partially immersed in the retinal layer, and some wrinkles were generated on the boundary between the MFs and the retinal layer, which greatly increased the contact area of the MFs and the retinal layer, providing a good foundation for subsequent photoelectric stimulation. In contrast, smooth glass MSs were also attached to the retinal layer; however, partial immersion of the glass MSs and wrinkle generation on the boundary were not observed (Figure 5b). The flower-like structures of the $ZnIn_2S_4$/NGQD MFs promoted cell attachment and the formation of a close interface between the $ZnIn_2S_4$/NGQD MFs and the retinal layer.

The WT mouse retina is organized into three main layers: the ONL with photoreceptors (rods and cones), the inner nuclear layer (INL) with bipolar cells, and the ganglion cell layer (GCL) with RGCs. WT mouse retinas displayed 12–15 layers of photoreceptor soma in the ONL, whereas the P66 rd10 retinas lost almost all the photoreceptors (Figure 5c,d). However, the bipolar cell and RGC layers were intact in the P66 rd10 retinas. Both the implanted $ZnIn_2S_4$/NGQD MFs and fluorescent glass MSs were located in the outer retinal space, in place of degenerated cells, and had direct contact with bipolar cells in rd10 retinas (Figure 5e,f). Analysis of SEM images and Z-stack confocal microscopy images showed that $ZnIn_2S_4$/NGQD MFs and fluorescent glass MSs formed a layer range of 10–15 μm in the original ONL. The Implanted $ZnIn_2S_4$/NGQD MFs adhered quite well to the retinal layer with minor changes after 5 days of microinjection. Under light stimulus without MF implantation, the spontaneous firing of certain RGCs was virtually absent in degenerative retinas compared with normal WT retinas (Figure 5g,h). Under the light stimulus, $ZnIn_2S_4$/NGQD implanted retinas and restored spontaneous spiking activity in the degenerative retinas, while no spiking activity was observed for glass MSs (Figure 5i,j). The above results demonstrate that the implanted $ZnIn_2S_4$/NGQD MFs can form a close interface in the degenerative retina to effectively restore the spiking activity of degenerative retinas. As controls, implants of glass MSs indicated by pink photoluminescence showed no light response, which was similar to the response of rd10 degenerative retinas (Figure 5d,f). To investigate the optimized dose of $ZnIn_2S_4$/NGQD MFs injection for restoring light response, MFs with various concentrations were tested in degenerative retinas (Figure S17, Supporting Information). It was observed that 4 mg mL^{-1} $ZnIn_2S_4$/NGQD MFs microinjection could induce the maximal light response in degenerative retinas, which was then applied in the following electrophysiology experiments. However, the number of light-responsive RGC decreased with a further increase in $ZnIn_2S_4$/NGQD MFs concentration in degenerative retinas. This may be explained by the excessive stimulation of $ZnIn_2S_4$/NGQD MFs to generate the interference of signaling. Excessive photocurrent stimulation generated by higher concentrations of $ZnIn_2S_4$/NGQD MFs may trigger potent lateral inhibition of the retina. In addition, an overly dense accumulation of microparticles may block and scatter the light projected onto the beads that have direct contact with the dendrites of bipolar cells. Furthermore, in order to provide a more comprehensive response to the reviewer's inquiry

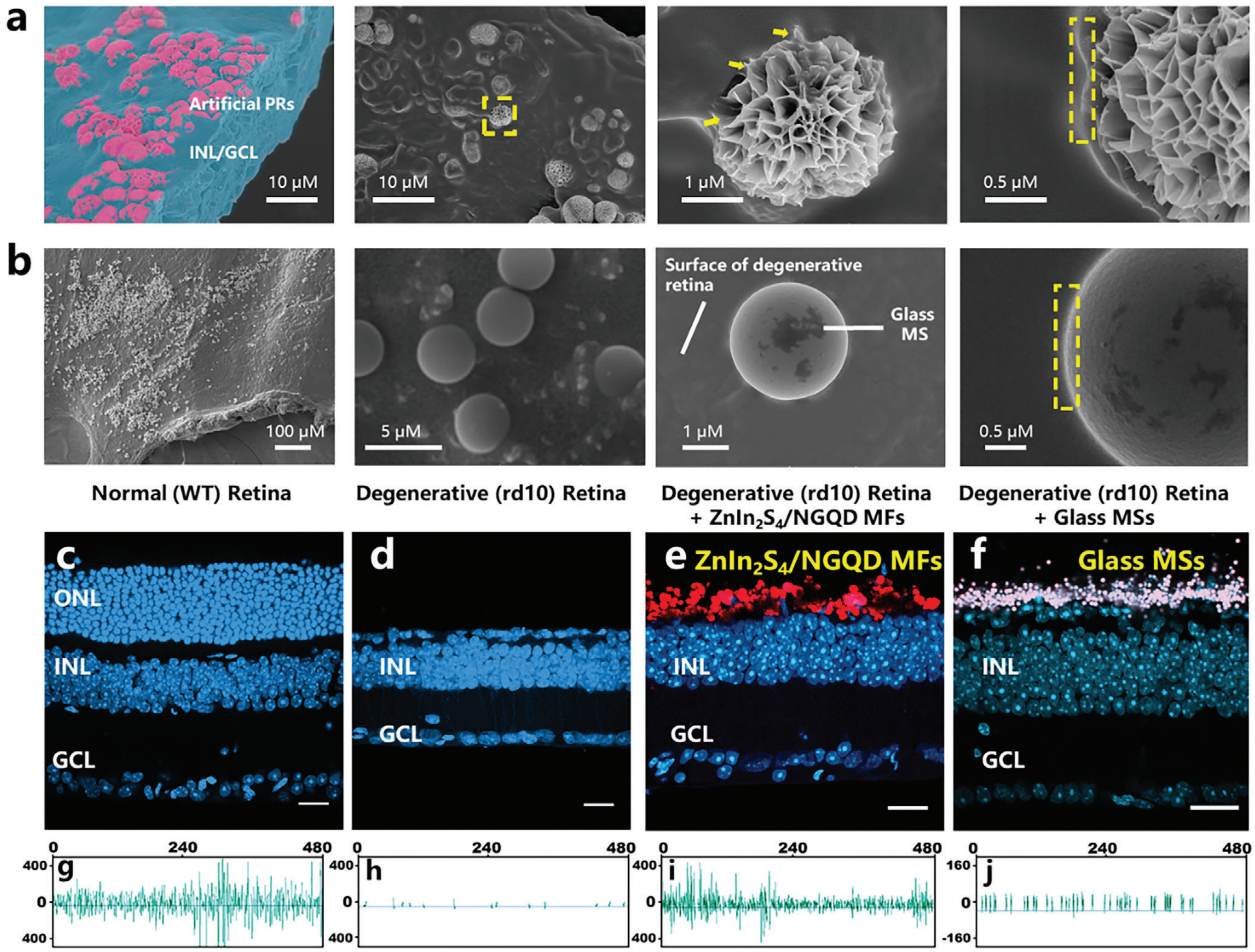

Figure 5. Subretinally microinjected $ZnIn_2S_4$/NGQD MFs displayed stable and close contact with retina and are not cleared over time. a) SEM images of $ZnIn_2S_4$/NGQD MFs on retinal layer. b) SEM images of the formation of glass MSs on the retina layer; c) Vertical section of the DAPI-staining for WT P66 mouse retina and d) P66 rd10 mouse retina. Photoreceptors with a 12–15 layer of soma were observed in the outer nuclear layer (ONL). Only one layer of soma of cells (possible surviving photoreceptors) was observed in the P66 rd10 mouse retina. Scale bar: 20 μm. e) DAPI-staining of the vertical section of P66 rd10 mouse retina with $ZnIn_2S_4$/NGQD MFs (red fluorescence) implanted in the ONL. Scale bar: 20 μm. f) Vertical section of the DAPI-staining for P66 rd10 mouse retina with glass MSs (pink fluorescence) implanted in the ONL. Scale bar: 20 μm, Light evoked firing of P66 WT mouse retina (g), P66 rd10 mouse retina (h), P66 rd10 mouse retina implanted with $ZnIn_2S_4$/NGQD MFs (i) and P66 rd10 mouse retina implanted with glass MSs (j) (X-axis: latency time with unit of millisecond; Y-axis: frequency of light-evoked firing of RGCs).

regarding the dose-dependent nature of the response, we have also performed an experiment to show the ability of RGCs injected with MF particles to respond to varying light intensities (Figure S18, Supporting Information). As the light intensity was incrementally increased from 13.9 Rh*/rod/sec to approximately 2 log units higher, we observed the emergence of ON responses characterized by a latency of approximately 0.5 s (indicated by the red star).

2.4. Visual Information Patterns of RGCs in P66 Rd10 Mice Retina Stimulated by $ZnIn_2S_4$/NGQD MFs

The biophysical properties of RGCs in degenerative retinas photostimulated with $ZnIn_2S_4$/NGQD MFs were studied. RGCs are the final output neurons from the retina to the brain. The retina of mice contains around 40 kinds of RGCs that code for distinctive visual input and transmit the visual scenes to the brain.[33] ON or OFF responses, which encode the onset and offset of light, are the most important feature for RGCs to code visual information.[34] These RGCs receive signal inputs from bipolar cells and inhibition inputs from amacrine cells (ACs) through conventional synapses.[35] Then different types of RGCs organize and integrate visual signals to higher brain centers.[36] Selective stimulation of ON/OFF cells is deemed crucial for restoring photoreceptor input and visual acuity, yet remains incompletely realized with current implantation technologies.[37]

Firing RGCs ($n = 740$ cells from 21 P66 rd10 retina; $n = 1804$ cells from 21 WT mice retinas) were recorded using a 256-channel microelectrode array (MEA) (Figure S19, Supporting Information). According to their light-evoked activities in response to square wave stimuli (525 nm full field, I = 1311

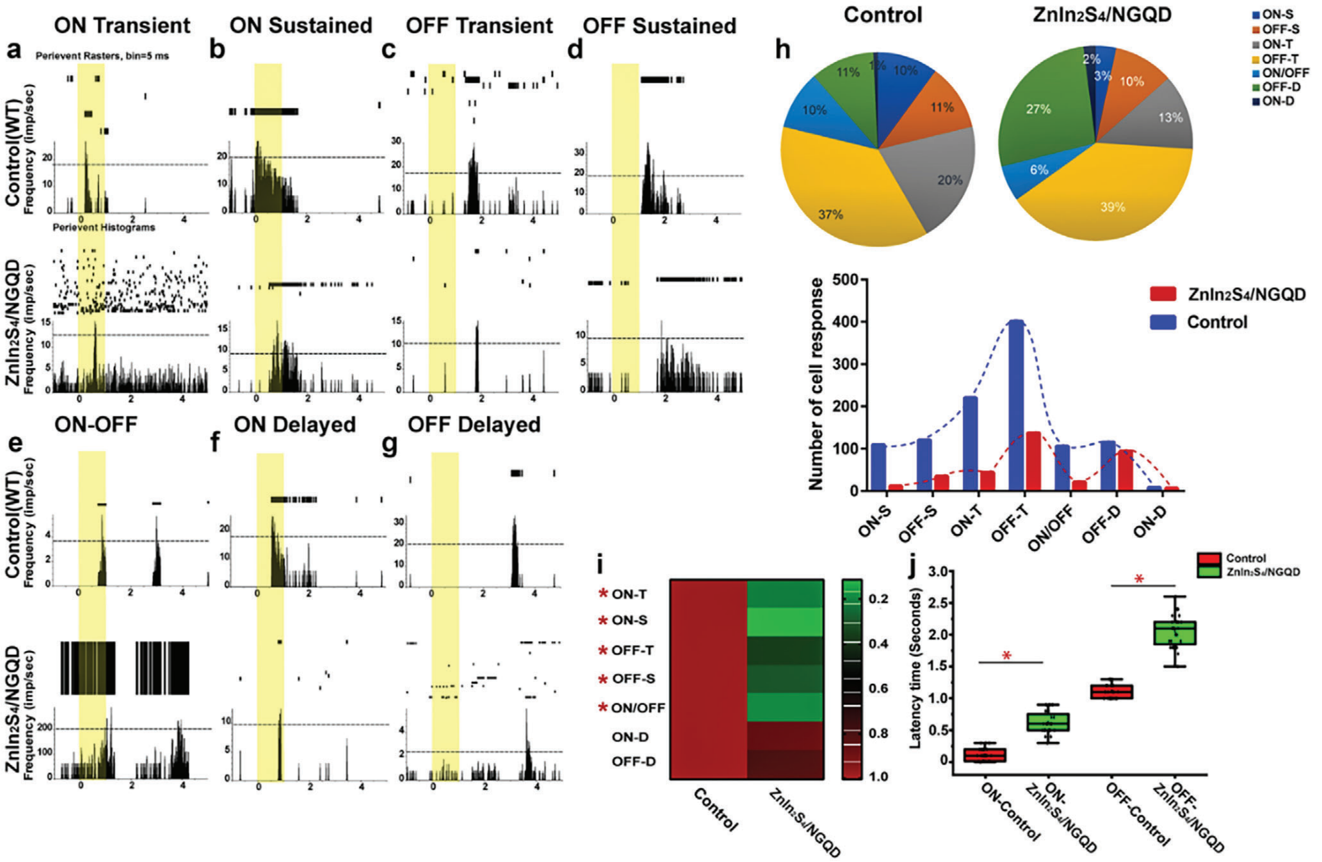

Figure 6. Visual information patterns of RGCs in degenerative mouse retina stimulated by $ZnIn_2S_4$/NGQD MFs. Raster plots and peristimulus time histograms (PSTHs) collected from a multi-electrode array (MEA) recording were compared between RGCs in degenerative mouse retinas implanted with $ZnIn_2S_4$/NGQD MFs and WT mouse retinas. a) ON transient (ON-T) RGC, b) ON sustained (ON-S) RGC. c) OFF transient (OFF-T) RGC. d) OFF sustained (OFF-S) RGC. e) ON-OFF RGC (ON/OFF). f) ON-Delayed RGC (ON-D) or displaced AC and g) OFF-Delayed RGC (OFF-D) or displaced AC. In graphs from a) to g), the raster plots were shown as distributed vertical bars in the upper part, and the PSTH were shown as histograms of frequency versus time in the lower part. In graphs from a) to g), the top shows RGC responses of normal WT mice retinas and Bottom shows RGC responses implanted with $ZnIn_2S_4$/NGQD MFs. 525 nm full-field (light intensity 1311 Rh*/rod/sec) 1 s light stimulus was applied. h) Top: Percentages of numbers for RGCs activated by $ZnIn_2S_4$/NGQD to the numbers of the same types of RGCs in WT mice. Bottom: Comparison of the distribution pattern of RGC cell response types between degenerative mouse retinas implanted with $ZnIn_2S_4$/NGQD MFs and WT mice retinas. i) Heatmap of normalized number in hand j) The latency time of light response of ON and OFF types of RGCs of the normal retina and degenerative retina implanted by $ZnIn_2S_4$/NGQD. $^*p < 0.01$.

photoisomerizations per rod per second, (Rh*/rod/second), 1-s stimulation, 5 intervals). ON and OFF RGCs were classified as cells that increased their spiking frequencies in response to either the light ON or OFF set. Then, sustained (maintained spiking) or transient (brief spike bursts) RGCs were further classified as previously described.[38] In addition, ON and OFF Delayed RGC types were also differentiated based on their delayed response kinetics with >0.3 s of latency, as previously reported.[39a,b] These RGC categories by MEA recordings might comprise mixed signals of RGC and displaced ACs. However, this had no impact on the overall signal observation of the firing patterns of cell populations.

The results demonstrated that the implanted $ZnIn_2S_4$/NGQD MFs could successfully photoactivate seven main types of RGCs in P66 rd10 degenerative retinas: ON Transient ($n = 220$ WT/44 rd10), ON Sustained ($n = 109$ WT/12 rd10), OFF Transient ($n = 401$ WT/137 rd10), OFF Sustained ($n = 120$ WT/35 rd10), ON-OFF ($n = 103$ WT/21 rd10), ON Delayed ($n = 8$ WT/7 rd10) and OFF Delayed ($n = 115$ WT/94 rd10) (**Figure** 6a–h, lower panel). The percentage of each type of RGCs activated by $ZnIn_2S_4$/NGQD MF to the same type of RGCs in WT mice was analyzed and compared as follows: ON Transient (20% in WT; 17% in rd10); ON Sustained (10% in WT; 3% in rd10); OFF Transient (37% in WT; 39% in rd10); OFF Sustained (11% in WT; 10% in rd10); ON-OFF (10% in WT; 6% in rd10); ON Delayed (1% in WT; 2% in rd10); and OFF Delayed (11% in WT; 27% in rd10) (Figure 6h, upper panel). Generally, the $ZnIn_2S_4$/NGQD MF-photoactivated RGCs showed a pattern similar to that of the normal retina (Figure 5h, lower panel). In particular, normalized RGCs showed that ON and OFF Delayed RGCs had no statistically significant difference in $ZnIn_2S_4$/NGQD MF-implanted rd10 retinas compared with WT retinas (Figure 6i). In contrast, ON/OFF Transient, ON/OFF Sustained, and ON-OFF RGCs had a statistically significant decrease in $ZnIn_2S_4$/NGQD MF-implanted rd10 retinas compared with WT retinas (Figure 6i). This indicated that the $ZnIn_2S_4$/NGQD-based MF biointerface

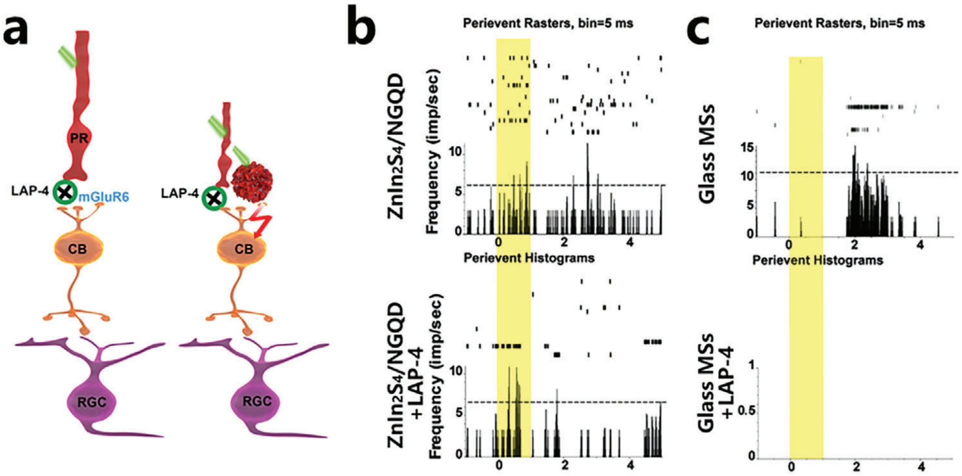

Figure 7. Visual stimulus signal transmittance pathway for $ZnIn_2S_4$/NGQD MFs-implanted RGCs. a) Schematic of synaptic transmittance from bipolar cell to ganglion cell in a normal WT retina and visual stimulus signal transmittance from $ZnIn_2S_4$/NGQD MFs to retina ganglion cell (RGC) in a degenerative rd10 retina. The ON pathway for transmission between photoreceptors and ON bipolar cells is blocked when treated with the mGluR6 agonist L-AP4 (left); In the degenerative retina implanted with $ZnIn_2S_4$/NGQD MFs, the ON pathway-induced response from residue photoreceptors is blocked in the presence of L-AP4. $ZnIn_2S_4$/NGQD MF can still photo-electrically stimulate cone bipolar cells and then activate RGCs. b) Light-evoked spiking activity of degenerative retina implanted with $ZnIn_2S_4$/NGQD MFs treated with L-AP4 (Top); Light-evoked spiking activity of degenerative retina treated with L-AP4 as control (Bottom) c) Light-evoked spiking activity of degenerative retina implanted with glass microspheres treated with L-AP4 (Top); Light evoked spiking activity of degenerative retina treated with L-AP4 as control (Bottom).

could photoactivate the ON- and OFF-Delayed RGCs more efficiently than the other types of RGCs. The successful photoactivation of the main types of RGCs with a pattern similar to that of the normal retina indicates the potential clinical application of this bionic interface.

Finally, we compared the latency time of ON and OFF RGCs in $ZnIn_2S_4$/NGQD MF-implanted rd10 and WT retinas. The latency time is defined as the time of spike generation after the light pulse, which could reflect the response kinetics of RGCs to stimulation.[10a] The latency time of ON-induced light responses displayed a statistically significant increase in the $ZnIn_2S_4$/NGQD MF-implanted rd10 retina (0.62 ± 0.03 s, mean ± SEM; $p < 0.01$, $n = 32$) compared with ON RGCs in WT retinas (0.12 ± 0.02 millisecond, $p < 0.01$, $n = 32$). The longer latency time of ON RGCs in $ZnIn_2S_4$/NGQD MF-implanted retina probably reflects the temporal/spatial integration of photopotentials used to trigger RGC firing and the extensive reactivation of degenerative retina from external cell layer interfaced with $ZnIn_2S_4$/NGQD MFs.[5a,12a] $ZnIn_2S_4$/NGQD MF may also trigger a presynaptic stimulation toward the INL and undergo a synaptic transmittance process, resulting in a longer latency.[40] In addition, the decrease in latency of OFF-induced light response was observed in $ZnIn_2S_4$/NGQD MF-implanted rd10 retina (1.05 ± 0.04 s, mean ± SEM; $p < 0.01$, $n = 32$) compared with OFF RGCs in WT retinas (1.12 ± 0.02 s, $p < 0.01$, $n = 32$) (Figure 6j). Combined with morphological analysis, the results revealed that numerous stimulating locations formed at the MF biointerface, potentially leading to an anisotropic response of neurons in the INL.[10a]

The direct pathway of visual stimuli in the normal retina is generated from photoreceptor cells (rods and cones) to bipolar cells and is finally encoded in RGCs. In P66 rd10 degenerative retinas, a new pathway of visual stimuli should be generated from MF to bipolar cells and finally encoded in RGCs (**Figure** 7a). It is possible that a small number of surviving photoreceptors in degenerative retinas still function and transmit signals to RGCs through the inner retinal circuit. To confirm that the recorded light responses of RGCs in degenerative retinas were generated from $ZnIn_2S_4$/NGQD MFs and not by any surviving photoreceptors, a low dose (2 µM) of 2-Amino-4-phosphonobutyric acid (APB or L-AP4), a glutamate antagonist, was applied to block the ON pathway for transmission between photoreceptors and ON bipolar cells[41] In the degenerative retinas implanted with the MF biointerface, ON responses from bipolar cells were still stimulated by intense light to cone bipolar cell and finally delivered to RGCs (Figure 7b). This light-induced ON RGC response was not abolished by L-AP4 in the $ZnIn_2S_4$/NGQD MF-implanted rd10 retinas. Interestingly, the aberrant bursting activity of background noise was decreased ($n = 21$) after 2 µM L-AP4 application. Therefore, the light response of the degenerative retina was primarily due to the implanted $ZnIn_2S_4$/NGQD MFs. We studied whether the light response of RGCs was generated explicitly by $ZnIn_2S_4$/NGQD MFs rather than by any other material. Glass MSs of the same size as the $ZnIn_2S_4$/NGQD MFs were implanted into P66 rd10 mice retinas as controls ($n = 19$). A weak RGC response signal due to residual photoreceptors was recorded in the degenerative retina (Figure 7c, upper figure). The application of L-AP4 eliminated almost all light responses in rd10 retinas with glass MSs implantation (Figure 7c, lower panel). Therefore, the restored light-evoked spiking was an artificial light response transmitted by photostimulation of the $ZnIn_2S_4$/NGQD-based MF biointerface.

Whether $ZnIn_2S_4$/NGQD MF implantation could induce responses in single RGCs level in P66 rd10 retinas was explored. The $ZnIn_2S_4$/NGQD MFs were implanted and formed a biointerface with the remaining bipolar cells (**Figure** 8a). From the

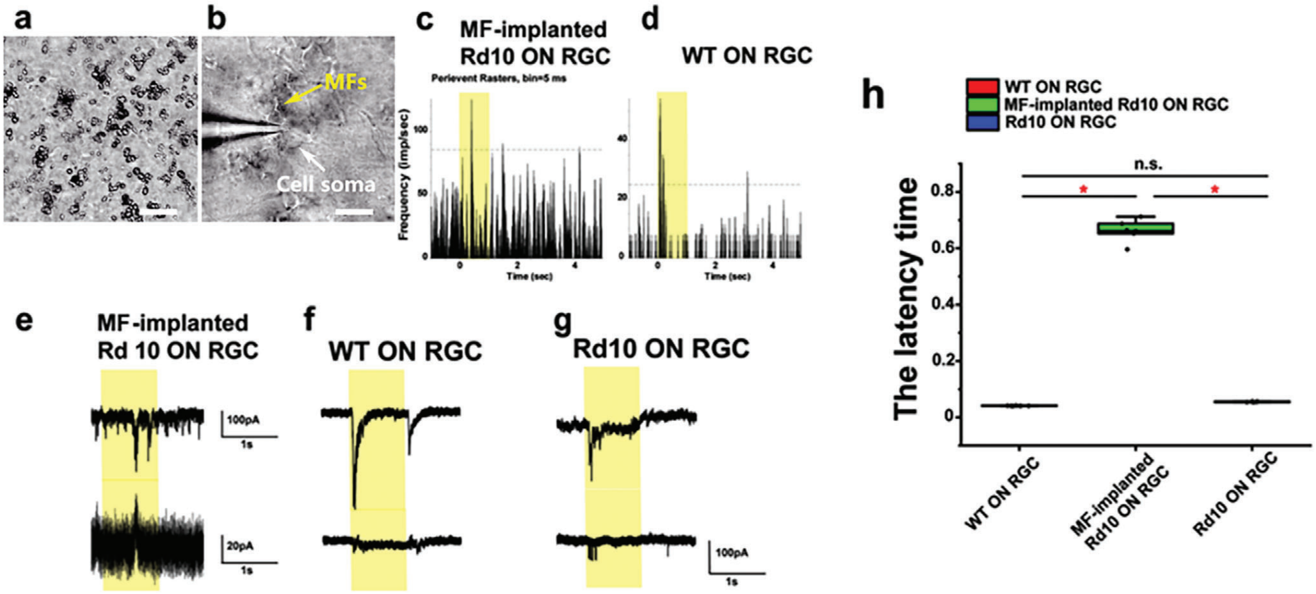

Figure 8. Patch recording in single ON RGC in $ZnIn_2S_4$/NGQD MF-implanted degenerative retina under a focal light spot. a) Bright-field microscopy images of RGC cells attached with MFs (Scale bar: 20 µm). b) The loose-cell patch and whole-cell patch recordings were performed on the RGC layer. Scale bar: 1 µm. c-d): The peristimulus time histogram of the ON RGC light responses with spike frequency in $ZnIn_2S_4$/NGQD MF-implanted degenerative retinas and WT retinas. e-g) EPSCs (upper parts) and IPSCs (lower parts) of ON RGCs from $ZnIn_2S_4$/NGQD MF-implanted degenerative retina, WT retina, and degenerative retinas. h) The comparison of latency time of EPSC currents of ON RGC among $ZnIn_2S_4$/NGQD MF-implanted degenerative retina, WT retina, and degenerative retinas.

photoreceptor side view of the whole-mount retina, the implanted $ZnIn_2S_4$/NGQD MFs were evenly spread on the surface of the retina with a density of 2.44×10^4 mm^{-2}. It is observed that a small collection of MFs were attached to the single RGC cell (Figure 8b, Figure S20, Supporting Information). Then, both the loose and whole-cell patches were applied to the RGC layer. The light response of ON RGC in the P66 rd10 mice retina implanted with $ZnIn_2S_4$/GQD MFs was successfully recorded with a focal light spot stimulation (125 µm diameter) (n = 15) (Figure 8c). The peri-stimulus time histogram of the ON RGC responses with spike frequency was calculated. The latency time of the ON RGC implanted with $ZnIn_2S_4$/GQD MFs was 0.583 s compared with the average of 0.04 s of the ON RGC in WT retinas (Figure 8c,d). To explore whether oscillation induced by $ZnIn_2S_4$/NGQD MF implantation had any difference in inhibition or excitation at the cellular level of RGCs, the excitatory postsynaptic currents (EPSCs) and inhibitory postsynaptic currents (IPSCs) of ON RGCs were examined by holding the membrane potential (Vh) on the levels matching either the excitatory (Vh = −68 mV) or the inhibitory reversal potentials (Vh = 0 mV) (Figure 8e–g). The latency times of EPSC currents of ON RGC in the retinas of the WT, rd10, and $ZnIn_2S_4$/NGQD MF-implanted rd10 groups were compared. The latency time of the light response in $ZnIn_2S_4$/NGQD MF-implanted rd10 retinas was 0.66 ± 0.02 s (n = 8) in excitatory currents from ON RGCs, whilst those in WT ON RGCs were 0.04 ± 0.001 s (n = 8) and 0.05 ± 0.001 s in the rd 10 retinas (n = 8). The increase in the latency time of ON RGCs in the $ZnIn_2S_4$/NGQD MF-implanted rd10 group was statistically significant ($p < 0.01$) (Figure 8h). In contrast, there was no significant difference between the retinas of WT and rd10 mice. Thus, the oscillation generated from $ZnIn_2S_4$/NGQD MF implantation reflects the photocurrent process at the single-cell level.

For the control, we subsequently tested the responses of RGCs in WT retina treated with MFs injection under various light intensities via patch clamp recording. The light responses in both ON (n = 5) and OFF (n = 5) RGCs exhibit normal characteristics, without the typical 0.5-s latency delay response observed in the light-triggered response from MF-treated rd retina (Figure S21, Supporting Information). This observation could be attributed to the intact retinal circuitry present in the WT retina. Since the MF particles contact the photoreceptors in WT mice rather than bipolar cells in the rd 10 mice, the additional electrical signal cannot bypass the normal circuitry. Furthermore, the synapses in the WT retinas, both chemical and electrical, remain intact, effectively filtering out most of the extraneous signaling induced by the MFs.

To evaluate the capability of $ZnIn_2S_4$/NGQD MFs for in vivo visual recovery, we performed a preliminary electroretinogram (ERG) test in P66 rd10 mouse with the subretinal injection of $ZnIn_2S_4$/NGQD MFs. The results showed that after subretinal injection of $ZnIn_2S_4$/NGQD MFs, the b-wave amplitude of the ERG response curve increased significantly at a luminance stimulus of −0.29 log cd×s m^{-2} (n = 4) (Figure S22a,b, Supporting Information). B-wave is generated when rod bipolar cells undergo depolarization. Therefore, the b-wave result demonstrated that the $ZnIn_2S_4$/NGQD MFs injection could significantly improve light responses in bipolar cells. Moreover, the amplitude of the positive scotopic threshold response (pSTR) was also measured by comparing the baseline to the highest peak of the waveform produced by the flash intensity. The p-STR is recognized as the most sensitive response in the ERG of dark-adapted individuals, which originates from the inner retina and

RGCs. It was observed that the p-STR was unrecordable before injection of $ZnIn_2S_4$/NGQD MFs and a recovery of pSTR response was generated after injection of $ZnIn_2S_4$/NGQD MFs at −4.32 log cd×s m^{-2} (Figure S22c,d, Supporting Information). The above in vivo ERG test demonstrated that subretinal injection of $ZnIn_2S_4$/NGQD MFs could significantly recover the degenerative retina function in the retina degenerative mouse model. More visual behavioral studies will be performed to further illustrate the potential for clinical application.

2.5. Discussion on Restoring the Light Responses of Degenerative Retinas by $ZnIn_2S_4$/NGQD MFs

In this study, we investigated the ability of $ZnIn_2S_4$/NGQD MFs to restore the light response of RGCs in degenerated rd 10 retinas. RGCs are the final output neurons of the vertebrate retina. Several aspects must be carefully considered to restore the light response of RGCs in degenerative retinas. First, $ZnIn_2S_4$/NGQD MFs induced light responses in the RGCs of rd10 retinas, depending on the intact function of the inner retinal circuit. Progression of neuronal and synaptic remodeling occurred from P30 to postnatal month 9.5. Following photoreceptor loss, plasticity progresses from the outer to the inner retina. It was reported that rod bipolar cell terminals exhibited a progressive decrease in size and ectopic connection with ACs and RGC by postnatal month 9.5, but the cone bipolar cell terminals retained appropriate synaptic function up to postnatal month 9.5.[42] In this study, the light restoration of RGCs could be recorded from P66 rd10 retinas, which indicated that function was intact in the inner retina. Therefore, the intact function of the inner retina is key for RGC light restoration in the rd10 retina. One attractive additional benefit of $ZnIn_2S_4$/NGQD MFs implantation for rd10 mice, as well as potentially for RP patients, is the possibility of delaying or even preventing the remodeling of second-order neurons and cell death by supplying synaptic input to those signal circuits. This has been confirmed in the early transplantation of differentiated photoreceptors and retinal stem cells.[43a,b]

Second, $ZnIn_2S_4$/NGQD MFs as artificial photoreceptors to induce light responses of RGCs need to be implanted at an appropriate concentration. Compared with the 12–15 layers of photoreceptors in WT retinas, P66 rd10 retinas had only one cell layer with an unknown function. $ZnIn_2S_4$/NGQD MFs implantation could pile up 2–3 layers in the original photoreceptor location, but only $ZnIn_2S_4$/NGQD MFs in direct contact with bipolar cells could trigger ectopically derived light responses. A concentration of 4 mg mL^{-1} was found to be the appropriate concentration for optimal effectiveness.

Third, the idea of restoring vision in neurodegenerative retinas began early in 1755 when Charles LeRoy induced visual perceptions of light by applying an electrical charge through the eye of a blind man.[44] By implanting retinal prosthetics on the retinal surface, damaged photoreceptors can be bypassed by electrically stimulating the surviving inner retinal neurons.[45] Implants in human patients can restore the preliminary perception of light and simple pattern recognition.[46] $ZnIn_2S_4$/NGQD MFs characterize photoelectric transduction ability. Bipolar cells in the inner retina can then be activated by direct extracellular electric stimuli generated by the $ZnIn_2S_4$/NGQD MFs. The light intensity induced by the light response of RGCs is approximately 1000 Rh* per rod/s. Compared with natural scenes, the present results show that stimulation of rd10 mice RGCs is safe, but the effect of the light intensity of stimuli, such as bright noon in the natural environment, requires further investigation. The latency in the $ZnIn_2S_4$/NGQD MF-induced RGCs response was 500 ms longer than the WT retinal light responses. These results imply that the implanted $ZnIn_2S_4$/NGQD MFs generate an additional delay between stimulus and perception in RGCs. This might be due to the photoelectrical transduction process in the $ZnIn_2S_4$/NGQD MFs. Spike-time precision is the key to visual information transmission to the brain.[47] The long-latency spikes would overlap spikes during natural firing patterns to decrease the ability to code visual information. Thus, the low temporal precision of the evoked spikes may not repetitively code light stimuli on a spike-by-spike basis. The $ZnIn_2S_4$/NGQD MFs may have a limited ability to code synchronized activity in RGCs.

The successful clinical application of $ZnIn_2S_4$/NGQD MFs in the treatment of RP relies on several important factors and requires further improvement. Initially, the intensity of the electrical stimulation must remain within safety thresholds and function in 2–3 log units of low light intensity, close to natural scenes, if possible. Second, the response to light stimulation should be close to the normal timing precision of retinal signals. Third, the spatial specificity of stimulation must be established and incorporated into the implanted $ZnIn_2S_4$/NGQD MFs.

3. Conclusion

Our findings demonstrate that implanted hybrid cell-like $ZnIn_2S_4$/NGQD microflowers in degenerative retinas can transfer light signals to electrical activity at the biointerface, acting as artificial photoreceptors and restoring light responses in seven major types of RGCs in P66 rd10 mice retinas. In these degenerative retinas, the number and distribution of the seven types of RGCs activated by $ZnIn_2S_4$/NGQD showed a pattern similar to that of the normal mice retina. Compared with wild-type retinas, the latency of the spikes in RGCs induced by $ZnIn_2S_4$/NGQD microflowers was 500 ms longer. As a proof-of-concept, the implanted MF biointerface indicates the desirability of bionic technology in visual rehabilitation. The development and application of $ZnIn_2S_4$/NGQD MFs, open up new possibilities for restoring visual function. However, the transition from experimental models to clinical applications necessitates a thorough exploration of how these microflowers can be optimized and integrated within a clinical setting. One of the primary considerations for clinical application is the biocompatibility and long-term stability of the $ZnIn_2S_4$/NGQD MFs. Modifications to the microflower design may include surface functionalization with biocompatible coatings to minimize potential immunogenicity and enhance integration with the surrounding retinal tissue. Additionally, the size and shape of the MFs could be tailored to optimize light absorption and electrical conductivity, ensuring efficient stimulation of the underlying bipolar cells. Integration strategies for clinical application also warrant careful consideration. The method of delivery of the MFs to the retinal surface plays a critical role in their effectiveness. Techniques such as minimally invasive injection or implantation through retinal surgery could be explored, with a focus on ensuring precise placement of the MFs in relation to the degenerated photoreceptors and bipolar cells. Furthermore, the development of a delivery system that allows for the controlled release of MFs over time could provide a sustained therapeutic effect and reduce the need for multiple interventions. Another aspect to consider is the interface between the $ZnIn_2S_4$/NGQD MFs and external light sources. For practical clinical application, the development of wearable or implantable devices that can provide the necessary light stimulation to the MFs is crucial. These devices should be designed to allow for adjustable light intensity and wavelength to cater to individual patient needs and to maximize the photoelectric response of the MFs. Finally, the long-term efficacy and safety of $ZnIn_2S_4$/NGQD MFs in a clinical setting must be rigorously evaluated through preclinical and clinical trials. This includes assessing the potential for any adverse effects, such as inflammation or rejection, and monitoring the functional restoration of vision over time.

In conclusion, while our study lays the groundwork for the use of $ZnIn_2S_4$/NGQD MFs in restoring light responses in PR-degenerative conditions, significant work remains to be done to translate this strategy into a viable clinical therapy. Detailed exploration of design modifications, integration strategies, and safety evaluations will be essential in moving forward. Through continued research and collaboration, we aim to bring this innovative approach closer to clinical reality, offering new hope for individuals affected by RP and similar conditions.

4. Experimental Section

Materials and Reagents: Indium (III) nitrate hydrate [In $(NO_3)_3$, 99.99% purity] was purchased from Thermo Fisher, Altringham, UK. Zinc nitrate hexahydrate [Zn $(NO_3)_2 \bullet 6H_2O$, 99%] from Xiya Reagent Co., Ltd., Shandung, China, and L-cysteine from Aladdin Chemical Co., Ltd., Shanghai, China. Milli-Q purified deionized water was used throughout the synthesis. All cell culture reagents, including Ham's F-12K medium, horse serum (HS), fetal bovine serum (FBS), phosphate-buffered saline (PBS), penicillin/streptomycin, and 0.25% trypsin ethylenediaminetetraacetic acid (EDTA) were obtained from Sigma-Aldrich (St. Louis, USA). Calcein AM/propidium iodide (PI) for live/dead cell staining was purchased from AAT Bioquest Inc., Sunnyvale, CA, USA, and the F-actin staining kit for super-resolution confocal imaging was purchased from Abcam, Cambridge, UK. The 200/30 iR-ITO-GR Multielectrode array (MEA) chamber was purchased from Multi Channel Systems, Reutlingen, Germany, and L-2-amino-4-phosphonobutyric acid (L-AP4) from Tocris Bioscience, Bristol, UK. Anti- Glial fibrillary acidic protein (GFAP) Mouse mAb, recombinant anti-IBA1 antibody (Mouse mAb), and citrate antigen retrieval solution were purchased from Wuhan Servicebio Technology Co., Ltd. TNF-α/IL-6 mouse uncoated enzyme-linked immunosorbent assay (ELISA) kits were purchased from the Thermo fisher scientific Inc. Type I rat tail collagen solutions were purchased from the Procell Life Sciences and Technology Co., Ltd.

Fabrication of $ZnIn_2S_{4/}$NGQD MF: NGQD was prepared based on a previous study.[16b] $ZnIn_2S_4$ microflowers with and without NGQD decoration were synthesized via a one-step hydrothermal reaction. For $ZnIn_2S_4$ microflowers synthesis, 0.25 mM Zn $(NO_3)_2$ and 0.5 mM $In(NO_3)_3$ were mixed by stirring in 30 mL deionized (DI) water. Then, 2 mM L-cysteine was added to the mixture with vigorous stirring and sonicated for 15 min. The mixture was then transferred into a Teflon-lined autoclave and held at 200 °C for 18 h for synthesis. $ZnIn_2S_4$ with irregular particle morphologies was prepared by collecting the products of the above mixtures at 0.5, 1, 4, 8, and 10 h. The reaction mixture was then cooled to room temperature and then washed by centrifuging at 12 000 rpm for 20 min 6 times with deionized water. The $ZnIn_2S_4$ microflowers were dried at 40°C for two days to obtain the powder for further use. For hybridized $ZnIn_2S_4$/NGQD microflowers synthesis, a further 1.5 mg NGQD were dispersed in 300 µL DI water via 10 min sonication and then added into a mixture of $Zn(NO_3)_2$, $In(NO_3)_3$, and L-cysteine with same ratio as above under vigorously stirring in 30 mL DI water. The products were collected using the procedure described above. $ZnIn_2S_4$ nanosheets were prepared according to the previously reported methods.[20b,28] 0.23 g $InCl_3$.4 H_2O, 0.05 g $ZnCl_2$, and 0.2 g thioacetamide were dissolved in 30 mL water, and then 0.2 g polyvinyl pyrrolidone (PVP) was added into the mixture. The mixture was vigorously stirred and followed by 10 min of sonication. Then the reaction mixture was kept for synthesis at 180 °C for 24 h. The final $ZnIn_2S_4$ product was collected by centrifugation under the same conditions as mentioned above.

$ZnIn_2S_4$/NGQD MF Characterization: Morphology and EDX elemental analyses of the $ZnIn_2S_4$ and $ZnIn_2S_4$/NGQD microflowers were performed using SEM (Tescan VEGA3, Tescan, Brno, Czechia). TEM images were obtained using a JEM-2100F electron microscope (JEOL, Tokyo, Japan). The ζ potentials and dynamic light scattering size distribution of $ZnIn_2S_4$ and $ZnIn_2S_4$/NGQD microflowers were determined at neutral pH by Zetasizer Nano (Anton Paar, Malvern, UK). The absorbance spectra of $ZnIn_2S_4$ and $ZnIn_2S_4$/NGQD powders were obtained using a UV-visible spectrophotometer (Shimadzu, UV-3600, Kyoto, Japan). The powder XRD patterns of the two materials were obtained using an X-ray diffractometer (Rigaku SmartLab, Tokyo, Japan). XPS was performed using a Thermo Scientific Nexsa System (Thermo Fisher Scientific, Waltham, Massachusetts, United States). The Electrochemical Impedance Spectroscopy (EIS) curve was characterized by CHI 660e electrochemical workstation within the frequency range of 0.1 to 10 000 HZ. The ultrafast transient absorption (TA) spectra of $ZnIn_2S_4$ materials were characterized by a femtosecond transient absorption system (Helio, Ultrafast System) with pump pulses at 350 nm and a probe range of 500–800 nm. Kelvin probe force microscopy (KPFM) imaging was obtained by using an atomic force microscope (Bruker, Dimension ICON).

Ethical Approval: All animal procedures were approved by the Animal Subjects Ethics Sub-Committee of the Hong Kong Polytechnic University and Animal Care (approval number: 18–19/79-SO-R-OTHERS). This study complied with the Guide for the Care and Use of Laboratory Animals published by the National Institutes of Health (eighth edition).

Animal Preparation: Adult rd10 mice (RRID: MGI: 3 581 193; B6.CXB1-Pde6brd10/J; Jackson Laboratory Stock No: 0 04297) were provided by Dr. Bin Lin, School of Optometry, The Hong Kong Polytechnic University. Adult rd10 mice (n = 40, postnatal day 66) and C57BL/6J (RRID: IMSR_JAX:000664) wild-type (WT) mice (n = 30 of either sex) were used in this study. P66 rd10 mice were used because all rods died after P38, and most of the cones were lost at P66. The animals were maintained in a 12–12 h day-night cycle. The mice were anesthetized with intraperitoneal injections of ketamine and xylazine [80 and 10 mg kg^{-1} (body weight), respectively], and lidocaine hydrochloride (20 mg mL^{-1}) was administered locally to the eyelids and surrounding tissue.

Flattened Retina Preparation: Retinas were explanted and dissected after microinjection of $ZnIn_2S_4$/NGQD microflowers. Since retinal activity of mice is higher in the evenings, all MEA experiments were carried out after 5 p.m. The eyeballs were taken out and sliced from the anterior segment to the ora serrata in a dim red light. Immediately following enucleation, the anesthetized animals were sacrificed by cervical dislocation. The anterior segment structure and vitreous and scleral tissues of the eyes were removed. The remaining retinal eyecup was placed in a superfusion chamber. The retinas were divided into four equal quadrants by radial dissection, and then they were flatly mounted on filter paper (8 µm pore size; Millipore, USA) for flat mounting. A similar method was used for the negative control group, in which 10 µL of glass microspheres were used. An RGC layer was placed toward the MEA electrodes to record signals. Details of these procedures have been previously published.[30]

SEM Characterization of $ZnIn_2S_4$/NGQD Interfaced Biosamples: The retina was acutely separated from one eye of the rd10 mice, and 4 mg mL^{-1} $ZnIn_2S_4$/NGQD microflowers were well dispersed in bicarbonate buffer and implanted into the ONL of the retina. The extracted retinal sample was fixed by a 2.5% glutaraldehyde solution in phosphate-buffered saline (PBS) for around 1 h at room temperature and gently washed twice with PBS. The samples were dehydrated using an ethanol solution with gradient concentrations of 20%, 40%, 60%, 95%, and 100%. The dehydration time was controlled at 10 min for each concentrated ethanol solution, and twice for fresh 100% ethanol (2 × 10 min). After drying at room temperature, the samples were sputtered by gold evaporation for imaging. For SEM imaging of the interfaces between $ZnIn_2S_4$/NGQD and PC12 cells, the cells were first cultured with $ZnIn_2S_4$/NGQD microflowers on a silicon wafer and processed according to the experimental protocol described above.

Photoelectric Measurement: The photoelectrochemical (PEC) current was measured using a CHI 760E electrochemical workstation (CH Instruments, Inc., Austin, TX, USA) with a standard three-electrode cell in a 0.1 M Na_2SO_4 electrolyte solution (pH 7.0). $ZnIn_2S_4$ or $ZnIn_2S_4$/NGQD was used as the working electrode and coiled Pt and Ag/AgCl were used as the counter and reference electrodes, respectively. The glass slides with Fluorine-doped Tin Oxide (FTO) coating (2 × 1 cm) were cleaned using ultrasonic waves in acetone, alcohol, and water for 15 min and then dried. Five milligrams of $ZnIn_2S_4$ or $ZnIn_2S_4$/NGQD were added to 1 mL of 0.5% DuPont Nafion solution (D520) and ultrasonicated for 20 min to obtain a uniform slurry. A 60 µL aliquot of the slurry was coated onto the FTO slide three times with an effective photoelectrode area of 1 cm^2 and was heated at 100 °C for 1 h. The photoanode samples, $ZnIn_2S_4$ or $ZnIn_2S_4$/NGQD were illuminated under a 520 ± 10 nm, 60 mW cm^{-2} of simulated light, which was produced by a PLS-SXE300D xenon lamp (Perfectlight, Beijing) with a monochromatic light filter and an GCI-71/GCI-73 M electronic timing shutter (Daheng Laser Equipment Co., Ltd, Beijing). The photogenerated current in each sample was measured over several on/off cycles under green illumination at a bias voltage of 0.5 V.

MEA Recording: Extracellular recording of the retinal RGCs from all retina quadrants was obtained using 256 channel multielectrode arrays (MEAs) (Multi Channel Systems Gmbh, Reutlingen, Germany), allowing recording from up to 252 retinal cells simultaneously. The electrodes were set up in a 16 × 16 grid (256MEA200/30iR-ITO). The electrode spacing of the 256 MEA electrodes was 200 µm and the diameter was 30 µm. The retina covered a 27.76 mm^2 area. By heating the bottom of the recording chamber and the inflowing fluid, the bathing temperature in the MEA was kept between 31 and 33 °C. To build the contact between the electrode and retina necessary to generate the spike and magnitude of the recorded spikes, retinal tissue was placed on the array for a minimum of 15–20 min before recording. Typically, during this time, the contact between the electrode and retina improved. Throughout the experiment, all of the data were concurrently recorded and saved for offline analysis. Digital recordings of spike trains were made using the MC Rack program (Multi Channel Systems Gmbh, Reutilingen, Germany) at a 20 kHz sampling rate. Additional offline analyses were conducted using NeuroExplorer (Nex Technologies, Littleton, MA, USA) and Offline Sorter (Plexon, Dallas, TX, USA). Principal component analysis was used to sort and time-stamp the spikes from the digital recordings (Offline Sorter, Plexon). Using Neuroexplorer software (Nex Technologies), peri-stimulus time histograms (PSTHs) and peri-raster raster histograms (5 ms bins) were produced from the time-stamped spike recordings of RGC pairs. Correlations exceeding 99% confidence intervals were used to establish the significance of associated spikes over chance. The background spike or current activity was subtracted from the number of lights that elicited ON and OFF spikes of RGCs or current amplitudes, respectively, by measuring the number of light stimulus start and offset.[30]

Patch-Clamp Recording: Extracellular recordings were collected for a single RGC in the mid-peripheral retina from the nasotemporal plane. Patch-clamp recordings were carried out by using an Axopatch 700B amplifier connected to a Digidata interface (1550B) and pCLAMP software (Version 10, Molecular Devices, San Jose, California, United States). To stimulate RGCs at the single-cell resolution level, we utilized a 40× objective lens with near-infrared illumination (>775 nm), resulting in a focal size close to the size of a single-cell soma. RGC was visualized via a Nuvicon tube camera (Dage-MTI, Michigan City, IN, USA) and differential interference optics with a fixed-stage microscope (Eclipse FN1; Nikon, Tokyo, Japan). Ringers solution was prepared with 120 NaCl, 25 $NaHCO_3$, 2.5 KCl, 2 $CaCl_2$, 1 $MgCl_2$, 0.1 NaH_2PO_4, 0.8 Na_2HPO_4, and 5 D-glucose (unit: mM). Retina slides were superfused in the Ringer solution with a rate of 1–1.5 mL min^{-1}. The bath solution of the slides was continuously bubbled with 5% CO_2 and 95% O_2 at 32 °C. The internal solution for electrodes was prepared with 10 HEPES, 12 KCl, 120 potassium gluconate, 5 EGTA, 1 $MgCl_2$, and 0.5 $CaCl_2$, and the pH was adjusted to 7.4 with KOH. The resistance of electrodes was pulled to 5−7 MΩ. This internal solution was applied in the recording when spiking was not blocked. During the perforated patch (with β-escin) or whole-cell recordings, in order to block spiking and improve the space clamp, the internal solution contained cesium methanosulfonate and 0.5 mM QX-314 instead of potassium gluconate. Absolute voltage values were acquired for an 11 mV liquid junction potential in the cesium-based intracellular solution. The excitatory and inhibitory currents were recorded at the chloride or cation equilibrium/reversal potentials of −68 and 0 mV, respectively. The digital recording of spike trains was conducted at a sampling rate of 10 kHz using Axoscope software and subsequently sorted using an offline sorter (Plexon) and NeuroExplorer (Nex Technologies) software.

Light Stimulation in Electrophysiologic Experiment: A green light-emitting diode ($\lambda = 525$ nm) provided consistent full-field visual stimuli to the retina's surface for the MEA experiment and a 125 µm diameter light spot generated by Mightex1000 for the patch recording. A light intensity of 1311 Rh*/rod/sec (equivalent to 94 µW cm^{-2}) was applied in retinal electrophysiology experiments to match the natural environmental brightness and to ensure effective activation of the cone pathway in the retina.[38,48] Using a portable radiometer/photometer, the intensity of the square-wave light stimuli was calibrated and expressed as the time-averaged photoisomerization rate per rod per second (Rh∗ per rod/sec). As previously published, light intensities were computed with an assumed average rod density of 437 000 rods mm^{-2} and a quantum efficiency of 0.67.

In Vivo Electroretinogram (ERG) Recordings: The animals were dark-adapted overnight to ensure retinal sensitivity. On the day preceding ERG recordings, the animals were subjected to inhalation anesthesia (3% isoflurane) under dim red light. Using 10 mg mL^{-1} tropicamide eye drops to dilate the mouse pupils, and 4 mg mL^{-1} benoxinate hydrochloride eye drops for local anesthesia of the mice. A 30-gauge needle was used to puncture the conjunctiva and then was connected to a Hamilton syringe to precisely control the flow of the MF dispersion. The MF was dispersed in a sterile saline solution and injected into the subretinal space at a rate of 200 nL s^{-1}, with a total injection volume of 2 µL. During microinjection procedures, a sterile saline solution was used to keep the mouse corneas moist. A full-filed Ganzfeld (Q450; RETI Animal, Roland Consult, Brandenburg a der Havel, Germany) was used to measure the ERG of Rd10 mice before and after the MF injection. Mice were dark-adapted overnight and anesthetized with an intraperitoneal injection of ketamine (100 mg kg^{-1} body weight) and xylazine (20 mg kg^{-1} body weight). Proxymetacaine (Provain-POS, Saarbrücken, Germany), tropicamide (5 mg mL^{-1} Mydrin-P, Santen Pharmaceutical, Osaka, Japan), and Carbomer gel (Lacryvisc, Alcon, Switzerland) were applied topically for anesthesia, pupil dilation, and corneal hydration. Subsequently, gold electrodes were placed on the corneas, while the ground electrode and reference electrode were placed on the mouse's tail and cheek area, respectively. Mice were stimulated with flashes of increasing intensity on a logarithmic scale (ranging from log −4.32–1.30 cd×s m^{-2}) and varying durations to record the retinal response waves. The signals were amplified and band-pass filtered from 0.2 to 30 Hz and 1 to 1000 Hz for scotopic threshold response (STR) and scotopic ERG, respectively. The amplitudes and latencies of the STR and a/b-wave were extracted over time.

Cell Culture and Biocompatibility Analysis: Mouse retinal pigment epithelial cells (RPECs) and the complete culture medium of RPECs (CM-M116) were purchased from Wuhan Pricella Biotechnology Co., Ltd. The complete medium contained Dulbecco's modified eagle medium (DMEM), glial cell growth supplement, insulin, 10% fetal bovine serum (FBS), and 1% antibiotic-antimycotic. Culture flasks were pre-coated with 12 µg mL^{-1} rat tail collagen I solutions for cell adhesion. Mouse retinal ganglion cells (661 W RGCs) were purchased from Shanghai YaJi Biotechnology Co., Ltd. The 661 W RGCs were cultured in F-12K medium and added with 10% FBS and 1% antibiotic-antimycotic. All cell cultures were maintained in the incubation at 37 °C with a humidified atmosphere and 5% CO_2. For the biocompatibility assay, cells were cultured with $ZnIn_2S_4$/NGQD for 24 and 48 h in a 6-well culture dish and then stained by the live/dead cell imaging reagent, Calcein AM/PI for 20 min at 37 °C. The cells were then imaged by the KEYENCE fluorescence microscope (BZ-X800). Cell viability was performed by using flow cytometry with excitation at 488 nm (CytoFLEX flow cytometer, Beckman). In the hemolysis assay, 1 mL blood samples of WT mice were collected and stabilized with ethylenediaminetetracetic acid. The blood samples were centrifugated for 10 min at 2000 rpm to separate the red blood cells (RBC). Then the RBC suspension was diluted with 10 mL PBS for a hemolysis test. 0.2 mL suspension was treated by PBS, deionized water, and 10–200 µg mL^{-1} $ZnIn_2S_4$/NGQD, respectively. The mixtures were shaken well and maintained at room temperature for 4 h and then centrifugated at 1000 rpm for 5 min. The absorbance value of each supernatant at 540 nm was measured by the UV-vis microplate reader. The hemolysis rate was calculated via the following equation: Hemolysis percentage (%) = (ODsample−ODnegative) / (ODpositive−ODnegative) × 100%. Serum samples of mice were isolated by centrifuging the blood with 3000 rpm for 15 min at 4 °C. TNF-α and IL-6 were quantitatively analyzed by ELISA kits according to the instructions. Optical density of samples was performed by the Biotek Epoch microplate reader, USA. Experimental measurements were performed in triplicates.

Histology and Immunocytochemistry: The dorsal region of the midperipheral retina in the nasotemporal plane was used to extract the retinas of mice. The retinal segments were separated from the eyecups and affixed with filter paper (RGCs up). They were then immersed in 4% paraformaldehyde in 0.1 M phosphate buffer (PBS, pH 7.5) for 30 min at room temperature. After fixing, the retinas were removed from the filter paper and thoroughly cleaned in 0.1 M PB (pH 7.4) in preparation for immunohistochemical examination. The mice's retinas were embedded in agarose gel and sections were cut using a vibratome (model LEICA VT 1200S; Leica Microsystems, Bannockburn, IL, USA) to examine the outer nuclear layer (ONL). Vectashield was used to mount the retinal slices on glass slides so they could be seen. Using 5 µM DAPI (Thermo Fisher Scientific) labeling, the soma of photoreceptor layers in the retinas of P66 rd10 and wild-type mice was demonstrated. To perform immunohistochemical analysis of GFAP and IBA1 on retinal slices, the slices were dried at 37 °C for 10 min and then incubated in a fixing solution for 30 min followed by three times washing with PBS (pH 7.4). Subsequently, the slices were treated for antigen retraveling. Briefly, the slices were treated with citrate buffer (pH 6.0) and subjected to microwave heating at medium power for 8 min, followed by a pause of 8 min, then switched to medium-low power for 7 min. The buffer solution should prevent excessive evaporation. The slices were naturally cooled, and then washed with PBS 3 times and blocked with 10% goat serum. Primary antibodies against GFAP and IBA1 markers were diluted in PBS containing 0.05% Triton X-100 and then incubated at 4 °C in a humidified chamber overnight. After incubation, retinal slices were washed with PBS (pH 7.4) 3 times and then incubated with a 1:100 dilution of the secondary antibodies for 1 h and DAPI dyes for 10 min. The slices were washed three times in PBS and then treated with spontaneous fluorescence quencher solution for 5 min. Retinal slices were finally mounted onto coverslips using an anti-fluorescence quenching mounting medium. GFAP intensity was quantitatively analyzed with Image J. Numbers of IBA1$^+$ cells were manually calculated in ONL. Retina morphometric images were obtained by using CaseViewer, 3DHISTECH's free slide viewing system, in Hungary. To evaluate the in vivo biocompatibility $ZnIn_2S_4$/NGQD MFs, WT mice were subretinal injected with 1 µL $ZnIn_2S_4$/NGQD dispersion. After 2 days of injection, the major organ tissues (kidney, heart, lung, liver, spleen) were extracted and maintained in paraffin for hematoxylin and eosin (H&E) staining. To analyze PR cell numbers, retinal slices were divided into 10 small regions with equal areas (5 ventral and 5 dorsal). PR numbers were simultaneously counted in each region. ONL thickness was analyzed by the ratio between the thickness of ONL and the total retina. Six areas were characterized for ONL thickness analysis.

Statistical Analysis: Statistical analyses were performed using the Origin software (OriginLab, Northampton, MA, USA). Statistical significance ($^*p < 0.05$, $^{**}p < 0.01$, $^{***}p < 0.001$, and $^{****}p < 0.0001$) was determined by using Student's t-test. The data shown are mean values ± standard error of the mean (SEM) unless specified otherwise.

Supporting Information

Supporting Information is available from the Wiley Online Library or from the author.

Acknowledgements

The research was supported by the Hong Kong Research Grants Council (RGC) General Research Fund (GRF) (15214619), the Hong Kong Research Grants Council (RGC) Early Career Scheme (ECS) (25103918), InnoHK initiative and the Hong Kong Special Administrative Region Government and the Hong Kong Research Grant Council Collaborative Research Fund (C5078-21EF). This study was supported by the Hong Kong Ph. D Fellowship Scheme (PF18-21168), and the Guangdong-Hong Kong Technology Cooperation Funding Scheme (GHP/032/20SZ and SGDX20201103095404018). This study was also supported by the Hong Kong Polytechnic University grants (UAG4, UAHA, UALC, CD6J, WZ4E, CD8M, and ZVVQ), the Hong Kong Polytechnic University Shenzhen Institute Bai Cheng Bai Yuan Fund (I2021A010 and I2022A002) and Shenzhen Municipal Science and Technology Innovation Commission Fund (JCYJ20210324130809025, JCYJ20230807093800001, and JCYJ20220531090808020). This work was supported by the Natural Science Foundation of China (22304120). The authors also thank the University Research Facility in Life Sciences (ULS) and University Research Facility in Behavioral and Systems Neuroscience (UBSN) for providing equipment and technical support.

Conflict of Interest

The authors declare no competing interests.

Author Contributions

G.O. and S.B. are the co-first authors of this article. G.O. designed and performed the artificial photoreceptor synthesis, characterization, and degenerative retina photostimulation experiments, processed and analyzed the material characterization data and biointerface imaging data, and wrote the main part of the original manuscript. S.B. Designed and performed the MEA recording experiments in a mouse model, processed and analyzed MEA data and wrote the MEA recording part, revised the original manuscript. Q.W. performed the patch clamp experiments and analyzed the patch clamp data. D. J. performed the characterization experiments of UV-vis diffusion spectra measurement; H. Wu performed the photocurrent measurement experiments. Y. Fan contributed to the data analysis of the SEM experiment. F.P. supervised the MEA and patch clamp experiments, provided conceptual input, designed the experiments, and revised the manuscript. M. Yang supervised the study, provided input for all of the experiments and the study concept, and edited the paper. All authors discussed, commented on, and revised the manuscript.

Data Availability Statement

Research data are not shared.

Keywords

biomimetic interface, degenerative retina, light response, photoelectronic interface, quantum dots

Received: January 12, 2024
Revised: May 30, 2024

[1] S. Ferrari, E. Di Iorio, V. Barbaro, D. Ponzin, F. S. Sorrentino, F. Parmeggiani, *Curr. Genomics* **2011**, *12*, 238.

[2] M. Chizzolini, A. Galan, E. Milan, A. Sebastiani, C. Costagliola, F. Parmeggiani, *Curr. Genomics* **2011**, *12*, 260.

[3] a) A. F. Wright, C. F. Chakarova, M. M. Abd El-Aziz, S. S. Bhattacharya, *Nat. Rev. Genet.* **2010**, *11*, 273; b) R. H. Masland, *Nat. Neurosci.* **2001**, *4*, 877.

[4] D. A. Prado, M. Acosta-Acero, R. S. Maldonado, *Curr. Opin. Ophthalmol.* **2020**, *31*, 147.

[5] a) Y. Mandel, G. Goetz, D. Lavinsky, P. Huie, K. Mathieson, L. Wang, T. Kamins, L. Galambos, R. Manivanh, J. Harris, D. Palanker, *Nat. Commun.* **2013**, *4*, 1980. b) K. Mathieson, J. Loudin, G. Goetz, P. Huie, L. Wang, T. I. Kamins, L. Galambos, R. Smith, J. S. Harris, A. Sher, D. Palanker, *Nat. Photonics* **2012**, *6*, 391; c) G. Xiao, Y. Song, Y. Zhang, Y. Xing, H. Zhao, J. Xie, S. Xu, F. Gao, M. Wang, G. Xing, X. Cai, *ACS Sens.* **2019**, *4*, 1992.

[6] a) J. A. Sahel, E. Boulanger-Scemama, C. Pagot, A. Arleo, F. Galluppi, J. N. Martel, S. D. Esposti, A. Delaux, J. B. de Saint Aubert, C. de Montleau, E. Gutman, I. Audo, J. Duebel, S. Picaud, D. Dalkara, L. Blouin, M. Taiel, B. Roska, *Nat. Med.* **2021**, *27*, 1223; b) J. A. Sahel, J. Bennett, B. Roska, *Sci. Transl. Med.* **2019**, 11; c) V. Busskamp, S. Picaud, J. A. Sahel, B. Roska, *Gene Ther.* **2012**, *19*, 169.

[7] a) A. Savchenko, V. Cherkas, C. Liu, G. B. Braun, A. Kleschevnikov, Y. I. Miller, E. Molokanova, *Sci. Adv.* **2018**, *4*, eaat0351; b) R. Yang, P. Zhao, L. Wang, C. Feng, C. Peng, Z. Wang, Y. Zhang, M. Shen, K. Shi, S. Weng, C. Dong, F. Zeng, T. Zhang, X. Chen, S. Wang, Y. Wang, Y. Luo, Q. Chen, Y. Chen, C. Jiang, S. Jia, Z. Yu, J. Liu, F. Wang, S. Jiang, W. Xu, L. Li, G. Wang, X. Mo, G. Zheng, et al., *Nat. Biomed. Eng.* **2023**, https://doi.org/10.1038/s41551-023-01137-8.

[8] a) A. Farnum, G. Pelled, *Front. Neurosci.* **2020**, *14*, 36; b) R. Parameswaran, J. L. Carvalho-de-Souza, Y. Jiang, M. J. Burke, J. F. Zimmerman, K. Koehler, A. W. Phillips, J. Yi, E. J. Adams, F. Bezanilla, B. Tian, *Nat. Nanotechnol.* **2018**, *13*, 260; c) S. Cupini, S. Di Marco, L. Boselli, A. Cavalli, G. Tarricone, V. Mastronardi, V. Castagnola, E. Colombo, P. P. Pompa, F. Benfenati, *ACS Nano* **2023**, 22800.

[9] a) Y. Jiang, J. L. Carvalho-de-Souza, R. C. Wong, Z. Luo, D. Isheim, X. Zuo, A. W. Nicholls, I. W. Jung, J. Yue, D. J. Liu, Y. Wang, V. De Andrade, X. Xiao, L. Navrazhnykh, D. E. Weiss, X. Wu, D. N. Seidman, F. Bezanilla, B. Tian, *Nat. Mater.* **2016**, *15*, 1023; b) D. Ghezzi, *Nat. Biomed. Eng.* **2020**, *4*, 137; c) J. F. Maya-Vetencourt, D. Ghezzi, M. R. Antognazza, E. Colombo, M. Mete, P. Feyen, A. Desii, A. Buschiazzo, M. Di Paolo, S. Di Marco, F. Ticconi, L. Emionite, D. Shmal, C. Marini, I. Donelli, G. Freddi, R. Maccarone, S. Bisti, G. Sambuceti, G. Pertile, G. Lanzani, F. Benfenati, *Nat. Mater.* **2017**, *16*, 681.

[10] a) V. Gautam, D. Rand, Y. Hanein, K. S. Narayan, *Adv. Mater.* **2014**, *26*, 1751; b) E. A. Rossi, A. Roorda, *Nat. Neurosci.* **2010**, *13*, 156; c) S. Francia, D. Shmal, S. Di Marco, G. Chiaravalli, J. F. Maya-Vetencourt, G. Mantero, C. Michetti, S. Cupini, G. Manfredi, M. L. DiFrancesco, A. Rocchi, S. Perotto, M. Attanasio, R. Sacco, S. Bisti, M. Mete, G. Pertile, G. Lanzani, E. Colombo, F. Benfenati, *Nat. Commun.* **2022**, *13*, 3677.

[11] B. Chen, L. Liu, K. Liu, F. Tong, S. Wang, D. Fu, J. Gao, J. Jiang, J. Ou, Y. Ye, D. A. Wilson, Y. Tu, F. Peng, *Adv. Funct. Mater.* **2020**, 31.

[12] a) L. Sawides, A. de Castro, S. A. Burns, *Vis. Res.* **2017**, *132*, 34; b) J. F. Maya-Vetencourt, G. Manfredi, M. Mete, E. Colombo, M. Bramini, S. Di Marco, D. Shmal, G. Mantero, M. Dipalo, A. Rocchi, M. L. DiFrancesco, E. D. Papaleo, A. Russo, J. Barsotti, C. Eleftheriou, F. Di Maria, V. Cossu, F. Piazza, L. Emionite, F. Ticconi, C. Marini, G. Sambuceti, G. Pertile, G. Lanzani, F. Benfenati, *Nat. Nanotechnol.* **2020**.

[13] a) C. Hao, Y. b. Tang, W. Shi, F. Chen, F. Guo, *Chem. Eng. J.* **2021**, *409*, 128168; b) G. Ma, C. Shang, M. Jin, L. Shui, Q. Meng, Y. Zhang, Z. Zhang, H. Liao, M. Li, Z. Chen, M. Yuan, X. Wang, C. Wang, G. Zhou, *J. Mater. Chem. C* **2020**, *8*, 2693.

[14] I. Gomaa, N. M. Hosny, M. A. Ibrahim, *J. Mol. Struct.* **2024**, 1296.

[15] M. Ali, R. Riaz, A. S. Anjum, K. C. Sun, H. Li, S. H. Jeong, M. J. Ko, *Carbon* **2021**, *171*, 493.

[16] a) D. Kong, X. Ruan, J. Geng, Y. Zhao, D. Zhang, X. Pu, S. Yao, C. Su, *Int. J. Hydro. Energy* **2021**, *46*, 28043; b) D. Jiang, C. Yang, Y. Fan, H. M. Polly Leung, K. Inthavong, Y. Zhang, Z. Li, M. Yang, *Biosens. Bioelectron* **2021**, *183*, 113214.

[17] A. Barriga-Rivera, L. Bareket, J. Goding, U. A. Aregueta-Robles, G. J. Suaning, *Front. Neurosci.* **2017**, *11*, 620.

[18] a) X. Jiao, Z. Chen, X. Li, Y. Sun, S. Gao, W. Yan, C. Wang, Q. Zhang, Y. Lin, Y. Luo, Y. Xie, *J. Am. Chem. Soc* **2017**, *139*, 7586; b) G. Yang, D. Chen, H. Ding, J. Feng, J. Z. Zhang, Y. Zhu, S. Hamid, D. W. Bahnemann, *Appl. Catal. B* **2017**, *219*, 611.

[19] J. Liu, H. Jung, A. Dubra, J. Tam, *Invest Ophthalmol. Vis. Sci.* **2018**, *59*, 4639.

[20] a) J. Wang, Y. Chen, W. Zhou, G. Tian, Y. Xiao, H. Fu, H. Fu, *J. Mater* **2017**, *5*, 8451; b) A. A. Khan, A. Molla, A. Chowdhury, S. Kumari, S. Hussain, *ACS Appl. Nano Mater.* **2021**, *4*, 4114.

[21] L. Wang, Z. Fan, F. Yue, S. Zhang, S. Qin, C. Luo, L. Pang, J. Zhao, J. Du, B. Jin, H. Zhang, *Food Chem.* **2023**, *430*, 137027.

[22] C. Liu, B. Chai, C. Wang, J. Yan, Z. Ren, *Int. J. Hydro. Energy* **2018**, *43*, 6977.

[23] a) S. Peng, P. Zhu, V. Thavasi, S. G. Mhaisalkar, S. Ramakrishna, *Nanoscale* **2011**, *36*, 2602; b) Y. Xu, A. Yan, L. Jiang, F. Huang, D. Huang, G. Duan, F. Zheng, *J. Alloys Compd.* **2022**, *895*, 162504.

[24] T. Liu, L. Wang, X. Liu, C. Sun, Y. Lv, R. Miao, X. Wang, *Chem. Eng. J.* **2020**, *379*, 122379.

[25] W.-K. Chong, B.-J. Ng, X. Kong, L. Tan, L. Putri, S.-P. Chai, *Appl. Catal. B Environ.* **2023**, *325*, 122372.

[26] a) Y. Wang, D. Chen, Y. Hu, L. Qin, J. Liang, X. Sun, Y. Huang, *Sustain. Energ. Fuels* **2020**, *4*, 1681; b) Y. Gao, B. Xu, M. Cherif, H. Yu, Q. Zhang, F. Vidal, X. Wang, F. Ding, Y. Sun, D. Ma, Y. Bi, Z. Xu, *Appl. Catal. B Environ.* **2020**, *279*, 119403.

[27] J. Wan, L. Liu, Y. Wu, J. Song, J. Liu, R. Song, J. Low, X. Chen, J. Wang, F. Fu, Y. Xiong, *Adv. Funct. Mater.* **2022**, *32*, 2203252.

[28] W. Yang, L. Zhang, J. Xie, X. Zhang, Q. Liu, T. Yao, S. Wei, Q. Zhang, Y. Xie, *Angew. Chem. Int. Ed. Engl.* **2016**, *55*, 6716.

[29] Y. Yin, Q. Liu, D. Jiang, X. Du, J. Qian, H. Mao, K. Wang, *Carbon* **2016**, *96*, 1157.

[30] A. L. Lyubarsky, B. Falsini, M. E. Pennesi, P. Valentini, J. E. N. Pugh, *J. Neurosci.* **1999**, *19*, 442.

[31] a) P. García-Estrada, M. A. García-Bon, E. J. López-Naranjo, D. N. Basaldúa-Pérez, A. Santos, J. Navarro-Partida, *Pharmaceutics* **2021**, *13*, 701; b) L. Nimeskern, H. Martínez Ávila, J. Sundberg, P. Gatenholm, R. Müller, K. S. Stok, *J. Mech. Behav. Biomed. Mater.* **2013**, *22*, 12.

[32] R. Yang, L. Mei, Y. Fan, Q. Zhang, R. Zhu, R. Amal, Z. Yin, Z. Zeng, *Small Methods* **2021**, *5*, 2100887.

[33] T. Baden, P. Berens, K. Franke, M. Román Rosón, M. Bethge, T. Euler, *Nature* **2016**, *529*, 345.

[34] P. H. Schiller, J. H. Sandell, J. H. Maunsell, *Nature* **1986**, *322*, 824.

[35] J. B. Demb, J. H. Singer, *Annu. Rev. Vis. Sci.* **2015**, *1*, 263.

[36] M. Rivlin-Etzion, W. N. Grimes, F. Rieke, *Trends Neurosci.* **2018**, *41*, 224.

[37] J. M. Begeng, W. Tong, B. Rosal, M. Ibbotson, T. Kameneva, P. R. Stoddart, *ACS Nano* **2023**, *17*, 2079.

[38] S. Banerjee, Q. Wang, C. H. So, F. Pan, *Cells* **2020**, 9.

[39] a) Q. Wang, S. Banerjee, C. So, C. Qiu, H. C. Lam, D. Tse, B. Völgyi, F. Pan, *Faseb* **2020**, *34*, 15282; b) F. Pan, *Cells* **2019**, 8.

[40] L. Bareket, N. Waiskopf, D. Rand, G. Lubin, M. David-Pur, J. Ben-Dov, S. Roy, C. Eleftheriou, E. Sernagor, O. Cheshnovsky, U. Banin, Y. Hanein, *Nano Lett.* **2014**, *14*, 6685.

[41] J. Jacoby, Y. Zhu, S. H. DeVries, G. W. Schwartz, *Cell Rep.* **2015**, *13*, 2663.

[42] M. J. Phillips, D. C. Otteson, D. M. Sherry, *J. Comp. Neurol.* **2010**, *518*, 2071.

[43] a) R. E. MacLaren, R. A. Pearson, A. MacNeil, R. H. Douglas, T. E. Salt, M. Akimoto, A. Swaroop, J. C. Sowden, R. R. Ali, *Nature* **2006**, *444*, 203; b) R. E. MacLaren, R. A. Pearson, *Eye* **2007**, *21*, 1352.

[44] C. Sekirnjak, P. Hottowy, A. Sher, W. Dabrowski, A. M. Litke, E. J. Chichilnisky, *J. Neurosci.* **2008**, *28*, 4446.

[45] M. Javaheri, D. S. Hahn, R. R. Lakhanpal, J. D. Weiland, M. S. Humayun, *Ann. Acad. Med. Singap.* **2006**, *35*, 137.

[46] D. Yanai, J. D. Weiland, M. Mahadevappa, R. J. Greenberg, I. Fine, M. S. Humayun, *Am. J. Ophthalmol.* **2007**, *143*, 820.

[47] M. J. Berry 2nd, M. Meister, *J. Neurosci.* **1998**, *18*, 2200.

[48] L. Yue, J. D. Weiland, B. Roska, M. S. Humayun, *Prog. Retin. Eye. Res.* **2016**, *53*, 21.